REMARKS ON CFD SIMULATION UNCERTAINTIES

Serhat Hosder, Bernard Grossman, Raphael T. Haftka,
William H. Mason, and Layne T. Watson

MAD Center Report 2003-02-01

**Multidisciplinary Analysis and Design Center
for Advanced Vehicles**

Virginia Polytechnic Institute & State University
Blacksburg, VA 24061-0203

REMARKS ON CFD SIMULATION UNCERTAINTIES

Serhat Hosder*, Bernard Grossman, Raphael T. Haftka,

William H. Mason, and Layne T. Watson

Multidisciplinary Analysis and Design (MAD) Center for Advanced Vehicles

Virginia Polytechnic Institute and State University

Blacksburg, VA 24061-0203, USA

Abstract

Different sources of uncertainty in CFD simulations are illustrated by a detailed study of 2-D, turbulent, transonic flow in a converging-diverging channel. Runs were performed with the commercial CFD code GASP using different turbulence models, grid levels, and flux-limiters to see the effect of each on the CFD simulation uncertainties. Two flow conditions were studied by changing the exit pressure ratio: the first is a complex case with a strong shock and a separated flow region, the second is the weak shock case with no separation. The uncertainty in CFD simulations has been studied in terms of five contributions: (1) iterative convergence error, (2) discretization error, (3) error in geometry representation, (4) turbulence model, and (5) the downstream boundary condition. In the discussion of the discretization error, results obtained from the RAE

---
*Corresponding author. Department of Aerospace and Ocean Engineering, 215 Randolph Hall, Virginia Polytechnic Institute and State University, Blacksburg, VA 24061-0203, USA. Phone: 1-540-2315956, Fax: 1-540-2319632, e-mail: shosder@vt.edu

2822 airfoil cases were also included as a representative study of the external flows. We show that for the simulation of attached flows, informed CFD users can obtain reasonably accurate results, whereas they are more likely to get large errors for the cases that have strong shocks with substantial flow separation. We demonstrate the difficulty in separating the discretization errors from physical modelling uncertainties originating from the use of different turbulence models in CFD problems that have strong shocks and shock-induced separation. For such problems, the interaction between different sources of uncertainty is strong, and highly refined grids, which would not be used in general applications, are required for spatial convergence. This study provides observations on CFD simulation uncertainties that may help the development of sophisticated methods required for the characterization and the quantification of uncertainties associated with the numerical simulation of complex turbulent separated flows.

Keywords: CFD, uncertainty, error, multidisciplinary design optimization

1   INTRODUCTION

Computational fluid dynamics (CFD) has become an important aero/hydrodynamic analysis and design tool in recent years. CFD simulations with different levels of fidelity, ranging from linear potential flow solvers to full Navier-Stokes codes, are widely used in the multidisciplinary design and optimization (MDO) of advanced aerospace and ocean vehicles [1]. Although low-fidelity CFD tools have low computational cost and are easily

used, the full viscous equations are needed for the simulation of complex turbulent separated flows, which occur in many practical cases such as high-angle-of attack aircraft, high-lift devices, maneuvering submarines and missiles [2]. Even for cases when there is no flow separation, the use of high-fidelity CFD simulations is desirable for obtaining higher accuracy. Due to modelling, discretization, and computation errors, the results obtained from CFD simulations have a certain level of uncertainty. It is important to understand the sources of CFD simulation errors and their magnitudes to be able to assess the magnitude of the uncertainty in the results.

Recent results presented in the *First AIAA CFD Drag Prediction Workshop* [3, 4] also illustrate the importance of understanding the uncertainty and its sources in CFD simulations. Many of the performance quantities of interest for the DLR-F4 wing-body configuration workshop test case, such as the lift curve slope, the drag polar, or the drag rise Mach number, obtained from the CFD solutions of 18 different participants using different codes, grid types, and turbulence models, showed a large variation, which revealed the general issue of accuracy and credibility in CFD simulations.

The objective of this work is to illustrate different sources of uncertainty in CFD simulations, by a careful study of typical, but complex fluid dynamics problems. We will try to compare the magnitude and importance of each source of uncertainty.

The main problem studied in this paper is a two-dimensional, turbulent, transonic flow in a converging-diverging channel. CFD calculations are done with the General Aerodynamic Simulation Program (GASP) [5]. Runs were performed with different turbulence

3

models, grid densities, and flux-limiters to see the effect of each on the CFD simulation uncertainties. In addition to these, the contribution of the error in geometry representation to the CFD simulation uncertainties is studied through the use of a modified geometry, based on the measured geometric data. The exit station of the diffuser and the exit pressure ratio are varied to determine the effects of changes of the downstream boundary conditions on the results. Besides the transonic diffuser case, observations on the discretization error of the flow simulations around the RAE 2822 airfoil are also presented. This article provides detailed information about the sources and magnitudes of uncertainties associated with the numerical simulation of flow fields that have strong shocks and shock-induced separated flows.

2   UNCERTAINTY SOURCES

To better understand the accuracy of CFD simulations, the main sources of errors and uncertainties should be identified. Oberkampf and Blottner [6] classified CFD error sources. In their classification, the error sources are grouped under four main categories: (1) physical modelling errors, (2) discretization and solution errors, (3) programming errors, and (4) computer round-off errors.

Physical modelling errors originate from the inaccuracies in the mathematical models of the physics. The errors in the partial differential equations (PDEs) describing the flow, the auxiliary (closure) physical models, and the boundary conditions for all the PDEs are

4

included in this category. Turbulence models used in viscous calculations are considered as one of the auxiliary physical models, usually the most important one. They are used for modelling the additional terms that originate as the result of Reynolds averaging, which in itself is a physical model.

Oberkampf and Blottner [6] define discretization errors as the errors caused by the numerical replacement of PDEs, the auxiliary physical models and continuum boundary conditions by algebraic equations. Consistency and the stability of the discretized PDEs, spatial (grid) and temporal resolution, errors originating from the discretization of the continuum boundary conditions are listed under this category. The difference between the exact solution to the discrete equations and the approximate (or computer) solution is defined as the solution error of the discrete equations. Iterative convergence error of the steady-state or the transient flow simulations is included in this category. A similar description of the discretization errors can also be found in Roache [7, 8], and Pelletier *et al.* [9].

Since the terms *error* and *uncertainty* are commonly used interchangeably in many CFD studies, it will be useful to give a definition for each. Uncertainty, itself, can be defined in many forms depending on the application field as listed in DeLaurentis and Mavris [10]. For computational simulations, Oberkampf *et al.* [11, 12] described *uncertainty* as a potential deficiency in any phase or activity of modelling process that is due to the lack of knowledge, whereas *error* is defined as a recognizable deficiency in any phase or activity of modelling and simulation.

Considering these definitions, any deficiency in the physical modelling of the CFD activities can be regarded as *uncertainty* (such as uncertainty in the accuracy of turbulence models, uncertainty in the geometry, uncertainty in thermophysical parameters *etc.*), whereas the deficiency associated with the discretization process can be classified as *error* [12].

Discretization errors can be quantified by using methods like Richardson's extrapolation or grid-convergence index (GCI), a method developed by Roache [8] for uniform reporting of grid-convergence studies. However, these methods require fine grid resolution in the asymptotic range, which may be hard to achieve in the simulation of flow fields around complex geometries. Also, non-monotonic grid convergence, which may be observed in many flow simulations, prohibits or reduces the applicability of such methods. That is, it is often difficult to estimate errors in order to separate them from uncertainties. Therefore, for the rest of the paper, the term *uncertainty* will be used to describe the inaccuracy in the CFD solution variables originating from discretization, solution, or physical modelling errors.

3 TRANSONIC DIFFUSER CASE

3.1 Description of the physical problem

The major test case presented in this paper is the simulation of a 2-D, turbulent, transonic flow in a converging-diverging channel, known as the *Sajben Transonic Diffuser* in CFD validation studies [13]. The exit station is at $x/h_t = 8.65$ for the geometry shown at the top part of Figure 1, where h_t is the throat height. This is the *original* geometry used in the computations and a large portion of the results with different solution and physical modelling parameters are obtained with this version. The exit station is located at $x/h_t = 14.44$ for the other geometry shown in Figure 1. This *extended* geometry is used to study the effect of varying the downstream boundary location on the CFD simulation results. For both geometries, the bottom wall of the channel is flat and the converging-diverging section of the top wall is described by an analytical function of x/h_t defined in Bogar *et al.* [14]. In addition to these two geometries, a third version of the same diffuser (the *modified-wall* geometry) has been developed for this research and has been used in our calculations. This version has the same inlet and exit locations as the original geometry, but the upper wall is described by natural cubic splines fitted to the geometric data points that were measured in the experimental studies. Having observed the fact that the upper wall contour obtained by the analytical equation and the contour described by experimental data points are slightly different, the modified-wall geometry is used to find the effects of geometric uncertainty on the numerical results.

Despite the relatively simple geometry, the flow has a complex structure. The exit pressure ratio P_e/P_{0i} sets the strength and the location of a shock that appears downstream of the throat (Figure 2). In our studies, for the original and the modified-wall geometries, we define $P_e/P_{0i} = 0.72$ as the strong shock case and $P_e/P_{0i} = 0.82$ as the weak shock case. A separated flow region exists just after the shock at $P_e/P_{0i} = 0.72$. Although a nominal exit station was defined at $x/h_t = 8.65$ for the diffuser used in the experiments, the physical exit station is located at $x/h_t = 14.44$. In the experiments, P_e/P_{0i} was measured as 0.7468 and 0.8368 for the strong and the weak shock cases respectively at the physical exit location. Table 1 gives a summary of the different versions of the transonic diffuser geometry and exit pressure ratios used in the computations.

A large set of experimental data for a range of exit pressure ratios are available [14]. In our study, top and bottom wall pressure values were used for the comparison of CFD results with the experiment. Note that the diffuser geometry used in the experiments has suction slots placed at $x/h_t = 9.8$ on the bottom and the side walls to limit the growth of the boundary layer. The existence of these slots can affect the accuracy of the quantitative comparison between the experiment and the computation at the downstream locations.

3.2 Computational modelling

CFD calculations are performed with GASP, a Reynolds-averaged, three-dimensional, finite-volume, Navier-Stokes code, which is capable of solving steady-state (time asymptotic) and time-dependent problems. For this problem, the inviscid fluxes were calculated by an upwind-biased third-order spatially accurate Roe flux scheme. The minimum modulus (Min-Mod) and Van Albada's flux limiters were used to prevent non-physical oscillations in the solution. All the viscous terms were included in the solution and two turbulence models, Spalart-Allmaras [15] (Sp-Al) and k-ω [16] (Wilcox, 1998 version) with Sarkar's Compressibility Correction, were used for modelling the viscous terms.

The adiabatic no-slip boundary condition was used on the top and the bottom walls of the transonic diffuser geometry. At the inlet, a constant total pressure (P_{0i}) and temperature (T_{0i}) were specified (subsonic P_{0i}-T_{0i} inflow boundary condition in GASP). The static pressure was taken from the adjacent interior cell and the other flow variables were calculated by using isentropic relations. At the exit, the outflow boundary was set to a constant static pressure (P_e), while the remaining flow variables were extrapolated from the interior cells. To initialize each CFD solution, inflow conditions were used.

The iterative convergence of each solution is examined by monitoring the overall residual, which is the sum (over all the cells in the computational domain) of the L^2 norm of all the governing equations solved in each cell. In addition to this overall residual information, the individual residual of each equation and some of the output quantities are also

monitored.

The sizes and the nomenclature of the grids used in the computations are given in Table 2. Grid 2 (top) and Grid 2_{ext} (bottom) are shown in Figure 1. To resolve the flow gradients due to viscosity, the grid points were clustered in the y-direction near the top and the bottom walls. In wall bounded turbulent flows, it is important to have a sufficient number of grid points in the wall region, especially in the laminar sublayer, for the resolution of the near wall velocity profile, when turbulence models without wall-functions are used. A measure of grid spacing near the wall can be obtained by examining the y^+ values defined as

$$y^+ = \frac{y\sqrt{\tau_w/\rho}}{\nu}, \tag{1}$$

where y is the distance from the wall, τ_w the wall shear stress, ρ the density of the fluid, and ν the kinematic viscosity. In turbulent boundary layers, a y^+ value between 7 and 10 is considered as the edge of the laminar sublayer. General CFD practice has been to have several mesh points in the laminar sublayer with the first mesh point at $y^+ = O(1)$. In our study, the maximum value of y^+ values for Grid 2 and Grid 3 at the first cell center locations from the bottom wall were found to be 0.53 and 0.26 respectively. The grid points were also stretched in the x-direction to increase the grid resolution in the vicinity of the shock wave. The center of the clustering in the x-direction was located at $x/h_t = 2.24$. At each grid level, except the first one, the initial solution estimates were obtained by interpolating the primitive variable values of the previous grid solution to the new cell locations. This method, known as *grid sequencing*, was used to reduce the

number of iterations required to converge to a steady state solution at finer mesh levels.

It should be noted that grid levels such as g5, g4, and g4$_{ext}$ are more highly refined than those normally used for typical two-dimensional problems and well beyond what could be used in a three-dimensional flow simulation. A single solution on Grid 5 required approximately 1170 hours of total node CPU time on a SGI Origin2000 with six processors, when 10000 cycles were run with this grid. If we consider a three-dimensional case, with the addition of another dimension to the problem, Grid 2 would usually be regarded as a fine grid, whereas Grid 3, 4, and 5 would generally not be used.

4   RESULTS AND DISCUSSION

For the transonic flow in the converging-diverging channel, the uncertainty of the CFD simulations is investigated by examining the nozzle efficiency (n_{eff}) as a global output quantity obtained at different P_e/P_{0i} ratios with different grids, flux limiters (Min-Mod and Van Albada), and turbulence models (Sp-Al and k-ω). The nozzle efficiency is defined as

$$n_{eff} = \frac{H_{0i} - H_e}{H_{0i} - H_{es}}, \tag{2}$$

where H_{0i} is total enthalpy at the inlet, H_e the enthalpy at the exit, and H_{es} the exit enthalpy at the state that would be reached by isentropic expansion to the actual pressure at the exit. Since the enthalpy distribution at the exit was not uniform, H_e and H_{es} were obtained by integrating the cell-averaged enthalpy values across the exit plane. Besides

11

n_{eff}, wall pressure values from the CFD simulations are compared with experimental data.

In the transonic diffuser study, the uncertainty in CFD simulation results has been studied in terms of five contributions: (1) iterative convergence error, (2) discretization error, (3) error in geometry representation, (4) turbulence model, and (5) changing the downstream boundary condition. In particular, (1) and (2) contribute to the numerical uncertainty, which is the subject of the verification process; (3), (4), and (5) contribute to the physical modelling uncertainty, which is the concern of the validation process.

In our study, we have seen that the contribution of the iterative convergence error to the overall uncertainty is negligible. A detailed analysis of the iterative convergence error in the transonic diffuser case is given in Appendix A. The main observations on the other sources of uncertainties are summarized in Table 3.

4.1   The discretization error

In order to investigate the contribution of the discretization error to the uncertainty in CFD simulation results, we study the Sp-Al and k-ω cases separately. Grid level and flux-limiter affect the magnitude of the discretization error. Grid level determines the spatial resolution, and the limiter is part of the discretization scheme, which reduces the spatial accuracy of the method to first order in the vicinity of shock waves.

A qualitative assessment of the discretization error in nozzle efficiency results obtained

with the original geometry can be made by examining Figure 3. The largest value of the difference between the strong shock results of Grid 2 and Grid 4 is observed for the case with Sp-Al model and the Min-Mod limiter. For the weak shock case, the difference between each grid level is not as large as that of the strong shock case when the results obtained with the Sp-Al turbulence model are compared. Weak shock results in Figure 3 also show that the k-ω turbulence model is slightly better than the Sp-Al in terms of the discretization error for this pressure ratio. Non-monotonic behavior of the k-ω results can be seen for the strong shock case as the mesh is refined, whereas the same turbulence model shows monotonic convergence for the weak shock cases. The Sp-Al turbulence model exhibits monotonic convergence in both shock conditions.

Richardson's extrapolation technique has been used to estimate the magnitude of the discretization error at each grid level for cases that show monotonic convergence. This method is based on the assumption that f_k, a local or global output variable obtained at grid level k, can be represented by

$$f_k = f_{exact} + \alpha h^p + O(h^{p+1}), \tag{3}$$

where h is a measure of grid spacing, p the order of the method, and α the pth-order error coefficient. Note that Equation 3 will be valid when f is smooth and in the asymptotic grid convergence range. In most cases, the *observed* order of spatial accuracy is different than the nominal (theoretical) order of the numerical method due to factors such as the existence of discontinuities in the solution domain, boundary condition implementation, flux-limiters, *etc.* Therefore, the observed value of p should be determined and used in the

13

calculations required for approximating f_{exact} and the discretization error. Calculation of the approximate value of the observed order of accuracy $(\tilde{p})$ needs the solutions from three grid levels, and the estimate of the f_{exact} value requires two grid levels. The details of the calculations are given in Appendix B.

Table 4 summarizes the discretization error in n_{eff} results obtained with the original geometry. When the results at grid level g2 are compared, the Sp-Al, Min-Mod, and $P_e/P_{0i} = 0.72$ case has the highest discretization error (6.97%), while the smallest error (1.45%) is obtained with k-ω turbulence model at $P_e/P_{0i} = 0.82$. The finest grid level, g5 was used only for the Sp-Al, Min-Mod, strong shock case obtained with the original geometry. Table 9 in Appendix B gives the discretization error values of this case, which are less than 1% at grid level g5.

In Table 4, the observed order of accuracy $\tilde{p}$, is smaller than the nominal order of the scheme and its value is different for each case with a different turbulence model, limiter, and shock condition. The values of both $(\tilde{n}_{eff})_{exact}$ and $\tilde{p}$ also depend on the grid levels used in their approximations. For example, the $\tilde{p}$ value was calculated as 1.322 and 1.849 for the Sp-Al, Min-Mod, strong shock case with different grid levels (See Appendix B, Table 9). These nonintegral $\tilde{p}$ values indicate grid convergence has not yet occurred, so the approximation of the discretization error at each grid level by Richardson's extrapolation is inaccurate (the source of some uncertainty).

The difference in nozzle efficiency values due to the choice of the limiter can be seen in the results of Grid 1 and Grid 2 for the strong shock case and Grid 1 for the weak shock

case. The maximum difference between the Min-Mod limiter and Van Albada limiter occurs on Grid 1 with the Sp-Al model. The relative uncertainty due to the choice of the limiter is more significant for the strong shock case. For both pressure ratios, the solutions obtained with different limiters give approximately the same nozzle efficiency values as the mesh is refined.

Figure 4 shows the significance of the discretization uncertainty between each grid level. In this figure, the noisy behavior of n_{eff} results obtained with Grid 1 can be seen for both turbulence models. The order of the noise error is much smaller than the discretization error between each grid level, however this can be a significant source of uncertainty if the results of Grid 1 are used in a gradient based optimization.

When we look at Mach number values at two points in the original geometry, one, upstream of the shock ($x/h_t = -1.5$) and the other, downstream of the shock ($x/h_t = 8.65$, the exit plane), both of which are located at the mid point of the local channel heights (Figure 5), we see the convergence of Mach number upstream of the shock for all the cases. However, for the strong shock case, the lack of convergence downstream of the shock at all grid levels with the k-ω model can be observed. For the Sp-Al case, we see the convergence only at grid levels g3 and g4. For the weak shock case, downstream of the shock, the convergence at all grid levels with the k-ω model is also seen. At this pressure ratio, Sp-Al model results do not seem to converge, although the difference between each grid level is small. These results may again indicate the effect of the complex flow structure downstream of the shock, especially the separated flow region seen in the strong

shock case, on the grid convergence.

The discretization error analysis of the flow simulation around the RAE2822 airfoil is presented in Appendix C. The observations from this external flow study also indicate the fact that the flow structure has significant effect on the grid convergence. The solutions of external flow fields that have strong shocks and shock-induced separations may contain a significant amount of discretization uncertainty at typical grid levels used in most CFD applications.

4.2   Error in the geometry representation

The contribution of the error in geometry representation to CFD simulation uncertainties is studied by comparing the results of the modified-wall and the original geometry obtained with the same turbulence model, limiter, and grid level. Figure 6 gives the percent error distribution in y/h_t (difference from the analytical value) for the upper wall of the modified-wall geometry at the data points measured in the experiments. Natural cubic splines are fit to these data points to obtain the upper wall contour. The difference between the upper wall contours of the original and the modified-wall geometry in the vicinity of the throat location is shown in Figure 7.

The flow becomes supersonic just after the throat and is very sensitive to the geometric irregularities for both $P_e/P_{0i} = 0.72$ and 0.82. From the top wall pressure distributions shown in Figures 8 and 9, a local expansion/compression region can be seen around

$x/h_t = 0.5$ with the modified-wall geometry. This is due to the local bumps created by two experimental data points, the *third* and the *fifth* ones from the throat (Figure 7).

Since neither the wall pressure results obtained with the original geometry nor the experimental values have this local expansion/compression, the values of these problematic points may contain some measurement error. The locations of these two points were modified by moving them in the negative y-direction halfway between their original value and the analytical equation value obtained at the corresponding x/h_t locations. These modified locations are shown with black circles in Figure 7. The wall pressure results of the geometry with the modified experimental points (Figures 8 and 9) show that the local expansion/compression region seems to be smoothed, although not totally removed. One important observation that can be made from the same figures is the improvement of the match between the CFD results and the experiment upstream of the throat when the modified-wall geometry is used. Since the viscous effects are important only in a very thin boundary layer near the wall region where there is no flow separation, contribution of the Sp-Al or the k-ω turbulence models to the overall uncertainty is very small upstream of the shock for both $P_e/P_{0i} = 0.72$ and 0.82.

4.3 Evaluation with the orthogonal distance error

The quantitative comparison of CFD simulation results with the experiment can be done considering different measures of error. In the transonic diffuser case, we use the

orthogonal distance error E_n to approximate the difference between the wall pressure values obtained from the numerical simulations and the experimental data. The error E_n is defined as

$$E_n = \frac{1}{N_{exp}} \sum_{i=1}^{N_{exp}} d_i, \tag{4}$$

where

$$d_i = \min_{x_{inlet} \leq x \leq x_{exit}} \left[(x - x_i)^2 + (P_c(x) - P_{exp}(x_i))^2 \right]^{1/2}. \tag{5}$$

In equations (4) and (5), d_i represents the orthogonal distance between the ith experimental point and the $P_c(x)$ curve (the wall pressure obtained from the CFD calculations), P_{exp} is the experimental wall pressure value, and N_{exp} is the number of experimental data points used. Pressure values are scaled by P_{0i} and the x values are scaled by the length of the channel.

The error E_n was evaluated separately in two regions: upstream of the experimental shock location (UESL) and downstream of the experimental shock location (DESL). The details of E_n calculations can be found in Hosder *et al.* [17]. Table 5 lists the top wall scaled error $\hat{E}_n$ values obtained for UESL with the original geometry, different grids, turbulence models, and flux-limiters. Table 6 gives DESL results.

It can be seen from Table 5 that the results obtained with the Sp-Al and the k-ω turbulence models are very close, especially for the weak shock case, when the values at the grid level g4 are compared. For each P_e/P_{0i}, the small difference between the results of each turbulence model at the finest mesh level originate from the difference in the shock locations obtained from the CFD calculations. This again shows that a large fraction

of the uncertainty observed upstream of the shock (UESL) in the wall pressure values originates from the uncertainty in the geometry representation. The difference in $\hat{E}_n$ between each grid level for each turbulence model and P_e/P_{0i} is very small indicating that the wall pressure distributions upstream of the shock obtained at each grid level are approximately the same. In other words, grid convergence is achieved upstream of the shock and the discretization error in wall pressure values at each grid level is very small.

Recall that the experimental data also contains uncertainty originating from many factors such as geometric irregularities, difference between the actual P_e/P_{0i} and its intended value, measurement errors, heat transfer to the fluid, *etc.* We have discussed the error due to geometric irregularities in the previous section. In a way, this error in geometry representation can also be regarded as a part of the uncertainty in the experimental data. By evaluating the orthogonal distance error in two separate regions, DESL and UESL, we tried to approximate the contribution of the geometric uncertainty to the CFD results obtained with the original geometry. However, experimental wall pressure values may still have a certain level of uncertainty associated with the remaining factors.

4.4   Turbulence models

To approximate the contribution of the turbulence models to the CFD simulation uncertainties in the transonic diffuser case, $\hat{E}_n$ values calculated for the top wall pressure distributions downstream of the shock (DESL) (Table 6) at grid level g4 are examined.

19

By considering the results of the finest mesh level, the contribution of the discretization error should be minimized, although it is difficult to isolate the numerical errors completely from the physical modelling uncertainties, especially for the strong shock case.

The Sp-Al turbulence model is more accurate than the k-ω model for the strong shock case. In fact, the difference is significant, with k-ω giving the highest error of all the cases, which is larger than the Sp-Al error by a factor of 3.6. With the Sp-Al model, the orthogonal distance error gets smaller as the mesh is refined, while the k-ω model gives the largest error value at grid level g4. When compared to the error values presented in Table 5, for the strong shock, the uncertainty of the k-ω turbulence model is 3.7 times larger than the error due to the geometric uncertainty. On the other hand, the uncertainty of the Sp-Al model has approximately the same magnitude as the geometric uncertainty.

As opposed to the strong shock case, the k-ω turbulence model gives more accurate wall pressure distributions than the Sp-Al model when the weak shock results of grid g4 are compared (Table 6). The orthogonal distance error of Sp-Al is twice as big as that of the k-ω model. The minimum error for the Sp-Al model is obtained at grid level g2, while the wall pressure distributions of the k-ω model get closer to the experimental distribution as the mesh is refined. The results of the Sp-Al model show that the most accurate results are not always obtained at the finest mesh level. The error due to the geometric uncertainty is bigger than the uncertainty of the k-ω model by a factor of 2.6 in the weak shock case. The uncertainty of the Sp-Al model is slightly smaller than the

20

geometric uncertainty for the same shock condition.

4.5 Downstream boundary condition

The effect of the downstream boundary location variation on the CFD simulation results of the transonic diffuser case has been investigated by using the extended geometry, which has the physical exit station at the same location as the geometry used in the actual experiments. For the strong shock case, the runs were performed with the Sp-Al model and two P_e/P_{0i} ratios, 0.72 and 0.7468. The second pressure ratio is the same value measured at the physical exit station of the geometry used in the experiments for the strong shock case. The results obtained with the extended geometry were compared to the results of the original geometry.

Figure 10 shows the streamline patterns of the separated flow region obtained with different geometries and P_e/P_{0i} ratios in the strong shock case. The comparison of the separation bubble size is given in Figure 11. The separation bubble obtained with the extended geometry and $P_e/P_{0i} = 0.72$ is bigger and extends farther in the downstream direction compared to the other two cases. The separation bubbles obtained with the original geometry ($P_e/P_{0i} = 0.72$) and the extended geometry ($P_e/P_{0i} = 0.7468$) are approximately the same in size. These results are also consistent with the top wall pressure distributions given in Figure 12.

With the extended geometry and $P_e/P_{0i} = 0.72$, the flow accelerates more under the

21

separation bubble, and the pressure is lower compared to the other cases where the separation bubbles have smaller thickness. Moving the exit location further downstream increases the strength of the shock and the size of the separation region. As the shock gets stronger, its location is shifted downstream. On the other hand, increasing P_e/P_{0i} reduces the strength of the shock, and moves the shock location upstream.

4.6   Discussion of uncertainty on nozzle efficiency

We use nozzle efficiency as a global indicator of the CFD results in the transonic diffuser case and the scatter in the computed values of this quantity originates from the use of different grid levels, limiters, turbulence models, geometries, and boundary conditions for each shock strength case. A graphical representation of this variation is given in Figure 3. This figure shows a cloud of results that a reasonably informed user may obtain from CFD calculations. The numerical value of each point is presented in Table 7. We will analyze the scatter in nozzle efficiency results starting from grid level 2, since the coarse Grid 1 will not be used by those that have significant experience in performing CFD simulations. On the other hand, grid levels 3 and 4 would generally not be used in practical CFD applications, particularly in three dimensions, due to their computational expense.

For the purpose of determining the variation in nozzle efficiency in terms of a percent value, we use the g4, Sp-Al, Van-Albada result as the comparator. When we consider

the cases obtained with the original geometry, maximum variation for the strong shock condition is 9.9% and observed between the results of g2, k-ω, Min-Mod and g4, Sp-Al, and Van Albada. Maximum difference in the weak shock results is 3.8% and obtained between the results of g2, k-ω, Van Albada and g4, Sp-Al, and Min-Mod.

For each case with a different turbulence model and limiter, the variation between the results of g2 and g4 may be used to get an estimate of the uncertainty due to discretization error. The maximum variation for the strong shock is 5.7% and obtained with Sp-Al model and the Min-Mod limiter. For the weak shock case, the maximum difference is 3.5% and obtained with the same turbulence model and limiter.

We can approximate the relative uncertainty originating from the selection of different turbulence models by comparing the nozzle efficiency values obtained with the same limiter and the grid level. At grid level 4, the maximum difference between the strong shock results of Sp-Al and k-ω model is 9.2% and obtained with the Min-Mod limiter. For the weak shock case, the maximum difference at grid level 2 is 2.2%, and obtained with the same limiter. It should be noted that, at each grid level, relative uncertainty due to the turbulence models is different resulting from the interaction of physical modelling uncertainties with the numerical errors.

For the strong shock case, at each grid level, the difference between nozzle efficiency values of the original geometry and the results of the modified-wall geometry is much smaller than the variations originating from the other sources of uncertainty regardless of the turbulence model and the limiter used. On the other hand, this difference is notable

for the weak shock case and varies between 0.9% and 1.4%.

Nozzle efficiency values of the extended geometry show considerable deviation from the results of the original geometry at certain grid levels, when 0.7468 and 0.8368 are used as the exit pressure ratios for the strong and the weak shock cases, respectively. For the exit pressure ratio of 0.7468, the maximum difference is 1.8% and obtained with grid level 3. The maximum difference for the exit pressure ratio of 0.8368 is 6.9% and observed at grid level 4. The difference between the results of the original and the extended geometry is smaller when the exit pressure ratios of 0.72 and 0.82 are used. For the exit pressure ratio of 0.72, the maximum difference is 0.8% and observed at grid level 3. A maximum difference of 1.1% is obtained at grid level 2 for the exit pressure ratio of 0.82.

Main observations on the uncertainties in nozzle efficiencies are summarized in Table 8.

5 CONCLUSIONS

Different sources of uncertainty in CFD simulations are illustrated by examining a 2-D, turbulent, transonic flow in a converging-diverging channel at various P_e/P_{0i} ratios by using the commercial CFD code GASP. Runs were performed with different turbulence models (Sp-Al and k-ω), grid levels, and flux-limiters (Min-Mod and Van Albada). Two flow conditions were studied by changing the exit pressure ratio: the first one was a complex case with a strong shock and a separated flow region; the second was a weak shock case with attached flow throughout the entire channel. The uncertainty in the CFD sim-

24

ulation results was studied in terms of five contributions: (1) iterative convergence error, (2) discretization error, (3) error in geometry representation, (4) turbulence model, and (5) downstream boundary condition. In the discussion of the discretization error, results obtained from the RAE 2822 airfoil cases were also included as a representative study of external flows. For the transonic diffuser case, in addition to the original geometry used in the calculations, the contribution of the error in geometry representation to the CFD simulation uncertainties was studied through the use of a modified geometry, based on the measured geometric data. Also an extended version of the transonic diffuser was used to determine the effect of a change of the downstream boundary location on the results.

Overall, this paper demonstrated that for the simulation of attached flows, informed CFD users can obtain reasonably accurate results, whereas they are more likely to get large errors for the cases that have strong shocks with substantial separation.

Both internal and external flow examples show that grid convergence is not achieved with grid levels that have moderate mesh sizes. Shocks and shock-induced separations have significant effect on the grid convergence. The magnitudes of discretization errors were influenced by the physical (turbulence) models used.

In some cases, turbulence modelling uncertainties and discretizations errors may cancel each other, and the closest results to the experiment can be obtained at intermediate grid levels. This shows the strong interaction among different types of uncertainties.

In nozzle efficiency results, the range of variation for the strong shock case was much larger than that observed in the weak shock case. The discretization errors were up to 6% and the relative uncertainty originating from the selection of different turbulence models was as large as 9% for the strong shock case. For the weak shock case, nozzle efficiency values were more sensitive to the exit boundary conditions and associated error magnitudes were larger than those from other sources. The difference between the results from the original geometry and the extended geometry was as large as 7% when the exit pressure ratio of 0.8368 was used. The contribution of the error in geometry representation to the overall uncertainty in nozzle efficiency results was up to 1.5% for the weak shock case, whereas this contribution was negligible for the strong shock case.

This study provides observations on CFD simulation uncertainties that may help the development of sophisticated methods required for the characterization and quantification of uncertainties associated with the numerical simulation of turbulent separated flows.

6 ACKNOWLEDGEMENTS

APPENDICES

A   The Iterative convergence error

The convergence of each transonic diffuser case to a steady-state solution has been examined by using various L^2 norm residuals and the n_{eff} results. The overall residual and the residual of each equation were monitored at every iteration, whereas the n_{eff} results were checked at certain iteration numbers. Figure 13 shows the convergence history of the L^2 norm residual of the energy equation for the strong shock case obtained with the Sp-Al turbulence model and the original geometry. The convergence history of the residual, normalized by its initial value, is presented for both limiters and the grid levels g1, g2, g3, and g4. By examining this figure, it can be seen that the main parameter that affects the residual convergence of a solution is the flux-limiter. With the Min-Mod limiter, the residuals of Grid g2, g3, and g4 do not reach even one order of magnitude reduction while the same grid levels show much better residual convergence when the Van Albada limiter is used. For example, the residual of Grid 3 was reduced more than seven orders of magnitude when 10000 cycles were run with the Van Albada limiter. The same convergence behavior of the Min-Mod and the Van Albada limiter was observed for the residual of the other equations and the weak shock case. The k-ω turbulence model also exhibited the same convergence behavior for Min-Mod and Van Albada limiters at both shock conditions.

Although the use of the Min-Mod limiter causes poor L^2 norm residual convergence, this does not seem to affect the final results, such as the wall pressure values or the nozzle efficiencies. Figure 14 shows the convergence history of nozzle efficiency at different grid levels for the Sp-Al, Min-Mod, strong shock case obtained with the original geometry. The convergence can be seen qualitatively at all grid levels for this scale of n_{eff} axis. However, at a smaller scale, small oscillations have been observed in nozzle efficiency results of Grid g4 and g5 starting from iteration number 10000. The amplitude of the oscillations (the fluctuating component of the n_{eff}) were on the order of 10^{-4} after the iteration number 13000 for Grid g5. As will be seen in the next section, the magnitude of the discretization error is much higher compared to the order of the iterative convergence error, especially in the coarser grid levels.

Although a steady-state solution is sought for each case, the physical problem itself may have some unsteady characteristics, such as the oscillation of the shock wave, which is a common phenomena observed in the transonic flows. Hsieh and Coakley [18] studied the unsteady nature of the shock in the Sajben Diffuser geometry by changing the exit location. They used a physical time step of 2.77×10^{-6} seconds to resolve the time-dependent shock oscillations and wall pressures. In this study, time-dependent runs were performed with grid levels g2 and g3 by using a physical time step of 10^{-2} seconds and no change in nozzle efficiency values, thus no unsteady effects were observed at that time-scale. In this study, it may be more appropriate to consider the output variables such as the n_{eff} values or the wall pressures obtained from the steady-state CFD runs as

the mean time-averaged values of the corresponding quantities over a longer time-scale than the one used in typical Reynolds time-averaging.

B   Approximation   of   the   discretization   error by Richardson's extrapolation

A detailed description of the traditional grid convergence analysis methods, which include the formulations given below, are presented in Roy [19]. We can write equation 3 for the nozzle efficiency results at three grid levels, grid g4, g3, and g2 as

$$(n_{eff})_4 = (n_{eff})_{exact} + \alpha h_4^p + O(h_4^{p+1})$$

$$(n_{eff})_3 = (n_{eff})_{exact} + \alpha h_3^p + O(h_3^{p+1}) \tag{6}$$

$$(n_{eff})_2 = (n_{eff})_{exact} + \alpha h_2^p + O(h_2^{p+1})$$

where h_k is a measure of grid spacing at grid level k and p is the observed order of the spatial accuracy. Since coarser grids were obtained from the finest grid level by *grid halving*, we have a constant grid refinement factor

$$r = \frac{h_1}{h_2} = \frac{h_2}{h_3} = \frac{h_3}{h_4} = 2.0. \tag{7}$$

By using equations 6 and 7,

$$r^{\tilde{p}} + 1 = \frac{\varepsilon_{34} + \varepsilon_{23}}{\varepsilon_{34}} \tag{8}$$

can be determined. Here $\tilde{p}$ is the approximated value for p and ε_{23} and ε_{34} are defined as

$$\varepsilon_{23} = (n_{eff})_2 - (n_{eff})_3,$$

$$\varepsilon_{34} = (n_{eff})_3 - (n_{eff})_4.$$

From equation 8, the approximate value of the observed order of spatial accuracy can be obtained as

$$\tilde{p} = \frac{ln(\varepsilon_{23}/\varepsilon_{34})}{ln(r)}. \tag{9}$$

By using the n_{eff} results obtained at grid levels g3 and g4, we can approximate the $(n_{eff})_{exact}$ as

$$(\tilde{n}_{eff})_{exact} = (n_{eff})_4 - \frac{\varepsilon_{34}}{r^{\tilde{p}} - 1}. \tag{10}$$

Here $(\tilde{n}_{eff})_{exact}$ will generally be $(\tilde{p} + 1)$ order accurate. Note that formulations above are derived based on the assumption that the discrete solutions obtained from three grid levels converge monotonically as the mesh size is refined. In case of non-monotonic convergence, different methods should be used. Roy [19] presented a grid convergence analysis method and an error estimation technique for mixed-order numerical schemes which exhibit non-monotonic convergence.

Once the $\tilde{p}$ and $(\tilde{n}_{eff})_{exact}$ values are determined, the percent discretization error can be estimated. The log-log plots of the |discretization error (%)| vs. h obtained with the original geometry, different turbulence models, limiters, and P_e/P_{0i} ratios are given in Figures 15 and 16. These figures give a graphical representation of the results listed in Table 4. If all the grid levels are in the asymptotic grid convergence range, the

30

|discretization error (%)| vs. h for each case should be a line with a constant slope in a log-log plot. However since we use grid levels g2 ($h = 4$), g3 ($h = 2$), and g4 ($h = 1$) for the calculation of $\tilde{p}$, this condition will always be satisfied at these grid levels. Therefore the change in the slope of the line connecting the results of grid levels g2 and g1 ($h = 8$) may imply that grid level g1, which is the coarsest mesh used in the computations, does not lie in the asymptotic grid convergence range.

In Table 4, the observed order of accuracy $\tilde{p}$, which is also used in the $(\tilde{n}_{eff})_{exact}$ calculations, has been estimated by using the n_{eff} values from grid levels g2, g3, and g4. The approximate value of $(n_{eff})_{exact}$ has been calculated by using the n_{eff} values obtained at grid levels g3 and g4.

The values of both $(\tilde{n}_{eff})_{exact}$ and $\tilde{p}$ depend on the grid levels used in their approximations. In Table 9, discretization error for the Sp-Al, Min-Mod, strong shock case is presented at each grid level, including g5. The first row of this table gives the $\tilde{p}$ value calculated with the results of grids g2, g3, and g4, and the $(\tilde{n}_{eff})_{exact}$ value obtained by using the results of grids g3 and g4. In the second row, the $\tilde{p}$ value is approximated by using the grid levels g3, g4, and g5, and the $(\tilde{n}_{eff})_{exact}$ value is estimated by using the results from grid levels g4 and g5. The difference in $\tilde{p}$ is significant between each case.

C The discretization error analysis of an external flow problem

The external flow problem is the simulation of steady, 2-D, turbulent flow around the RAE 2822 airfoil (Figure 17). In this study, we present the discretization error results of two different flow conditions. In the first case, free-stream Mach number is 0.3 and the airfoil is at zero degrees angle of attack (α). For the second case, Mach Number is 0.75 and the angle of attack is increased to 3.19 degrees. Reynolds number (Re) is 6.2×10^6 for both flow conditions. In the first problem, whole flowfield is subsonic and there is no flow separation on the airfoil surface. The second case represents a more difficult CFD problem. Flowfield is transonic and a shock wave exists approximately at the mid-chord location of the airfoil upper surface. After the shock, there is a separated flow region. The thickness of this shock-induced separation region is much smaller than the one observed in the internal flow (transonic diffuser) case with strong shock.

The external flow simulations were also performed with GASP. The inviscid fluxes were calculated by an upwind-biased third-order spatially accurate Roe flux scheme with the Min-Mod limiter. Sp-Al turbulence model was used for modelling the viscous terms. Four grid levels were used in the calculations. The dimensions of these grids are given in Table 10. Figure 17 shows the second mesh level used in the computations.

The lift coefficients (CL) were calculated at all grid levels for each case (Table 10). Richardson's extrapolation was used to estimate the discretization error at each grid

level. As also seen in the transonic diffuser problem, the observed order of accuracy is different for each case. The complex flow problem with the shock and flow separation has a spatial accuracy of approximately first-order, and the other case has an order, which is slightly bigger than two. As can be seen from Figure 18, the grid convergence is achieved for the first case. The discretization error values at grid levels 3 and 4 are much smaller than the ones obtained for the second case. In fact, starting from grid level 3, which is the typical mesh size to be used in CFD applications, the discretization error becomes negligible.

The discretization error results obtained for the external flow problem are consistent with the observations on the internal flow simulations. The flow structure has significant effect on the discretization error. It becomes more difficult to achieve the grid convergence and the desired level of numerical accuracy as the flowfield gets more complicated with the presence of shock waves and shock-induced separations.

References

[1] Hosder, S., Watson, L. T., Grossman, B., Mason, W. H., Kim, H., Haftka, R. T., and Cox, S. E. "Polynomial Response Surface Approximations for the Multidisciplinary Design Optimization of a High Speed Civil Transport". *Optimization and Engineering*, **2**(4):431–452, 2002.

[2] Jameson A. and Martinelli L. "Mesh Refinement and Modeling Errors in Flow Simulation". *AIAA Journal*, **36**(5):676–686, May 1998.

[3] Levy, D. W., Zickuhr, T., Vassberg, J., Agrawal, S., Wahls, R. A., Pirzadeh, S., and Hemsch, M. J. "Summary of Data from the First AIAA CFD Drag Prediction Workshop", AIAA Paper 2002-0841, January 2002.

[4] Hemsch, M. J. "Statistical Analysis of CFD Solutions from the Drag Prediction Workshop", AIAA Paper 2002-0842, January 2002.

[5] *GASP User Manual*. AeroSoft, Inc., Blacksburg, Virginia, 1997.

[6] Oberkampf, W. L. and Blottner, F. G. "Issues in Computational Fluid Dynamics Code Verification and Validation". *AIAA Journal*, **36**(5):687–695, May 1998.

[7] Roache, P. J. "Quantification of Uncertainty in Computational Fluid Dynamics". *Annual Review of Fluid Mechanics*, **29**:123–160, 1997.

[8] Roache, P. J. *Verification and Validation in Computational Science and Engineering*. Hermosa Publishers, Albuquerque, New Mexico, 1998.

[9] Pelletier, D., Turgeon, E., Lacasse, D., and Borggaard, J. "Adaptivity, Sensitivity, and Uncertainty: Towards Standarts in CFD", AIAA Paper 2001-0192, January 2001.

[10] DeLaurentis D. A. and Mavris, D. N. "Uncertainty Modeling and Management in Multidisciplinary Analysis and Synthesis", AIAA Paper 2000-0422, January 2000.

[11] "Guide for the verification and Validation of Computational Fluid Dynamics Simulations". *AIAA Standard G-077-1998*, January 1998.

[12] Oberkampf, W. L. and Trucano, T. G. "Validation Methodology in Computational Fluid Dynamics", AIAA Paper 2000-2549, June 2000.

[13] Bush, R. H., Power, G. D., and Towne, C. E. "WIND: The Production Flow Solver of the NPARC Alliance", AIAA Paper 1998-0935, January 1998.

[14] Bogar, T. J., Sajben, M., and Kroutil, J. C. "Characteristic Frequencies of Transonic Diffuser Flow Oscillations". *AIAA Journal*, **21**(9):1232–1240, September 1983.

[15] Spalart, P. R. and Allmaras, S. R. "A One-Equation Turbulence Model for Aerodynamic Flows", AIAA Paper 1992-0439, January 1992.

[16] Wilcox, D. C. *Turbulence Modeling for CFD, 2nd Edition.* DCW Industries, La Canada, California, 1998.

[17] Hosder, S., Grossman, B., Haftka, R. T., Mason, W. H., and Watson, L. T. "Observations on CFD Simulation Uncertainties", AIAA Paper 2002-5531, September 2002.

[18] Hsieh T. and Coakley, T. J. "Downstream Boundary Effects on the Frequency of Self-excited Oscillations in Transonic Diffuser Flows", AIAA Paper 87-0161, January 1978.

[19] Roy, C. J. "Grid Convergence Error Analysis For Mixed-Order Numerical Schemes", AIAA Paper 2001-2006, June 2001.

List of Tables

List of Figures

42

Table 1: Different versions of the transonic diffuser geometry and exit pressure ratios (P_e/P_{0i}) used in the computations.

Geometry	x/h_t at the exit station	P_e/P_{0i}
original	8.65	0.72 and 0.82
modified-wall	8.65	0.72 and 0.82
extended	14.44	0.72, 0.7468 0.82, and 0.8368

Table 2: Mesh size nomenclature for the transonic diffuser case. In the simulations, five different grids were used for the original geometry: Grid 1 (g1), Grid 2 (g2), Grid 3 (g3), Grid 4 (g4), and Grid 5 (g5). The finest mesh is Grid 5 and the other grids are obtained by reducing the number of divisions by a factor of 2 in both x- and y-directions at each consecutive level (grid halving). Grid 5 is used only for the case with the Sp-Al turbulence model, Min-Mod limiter, and $P_e/P_{0i} = 0.72$. Four grid levels were used for the extended geometry: Grid 1_{ext} (g1$_{ext}$), Grid 2_{ext}, (g2$_{ext}$), Grid 3_{ext} (g3$_{ext}$), and Grid 4_{ext} (g4$_{ext}$). The grids for the extended geometry and the grids generated for the original geometry are essentially the same between the inlet station and $x/h_t = 8.65$. For the modified-wall geometry, three grid levels were used: Grid 1_{mw} (g1$_{mw}$), Grid 2_{mw} (g2$_{mw}$), and Grid 3_{mw} (g3$_{mw}$). All the grids have the same mesh distribution in the y-direction.

Grid	x/h_t at the exit station	mesh size
g1	8.65	$41 \times 26 \times 2$
g2	8.65	$81 \times 51 \times 2$
g3	8.65	$161 \times 101 \times 2$
g4	8.65	$321 \times 201 \times 2$
g5	8.65	$641 \times 401 \times 2$
g1$_{ext}$	14.44	$46 \times 26 \times 2$
g2$_{ext}$	14.44	$91 \times 51 \times 2$
g3$_{ext}$	14.44	$181 \times 101 \times 2$
g4$_{ext}$	14.44	$361 \times 201 \times 2$
g1$_{mw}$	8.65	$41 \times 26 \times 2$
g2$_{mw}$	8.65	$81 \times 51 \times 2$
g3$_{mw}$	8.65	$161 \times 101 \times 2$

Table 3: Main observations on uncertainty sources

Uncertainty sources	Observations
Discretization error	Both internal and external flow examples show that grid convergence is not achieved with grid levels that have moderate mesh sizes. When the flow-field includes shocks with substantial flow separation, highly refined grids, which are beyond the grid levels we use in this study, are needed for spatial convergence. Even with the finest mesh level we can afford, achieving asymptotic convergence is not certain. For the transonic diffuser case, the discretization error magnitudes are different for cases with different turbulence models, when nozzle efficiency results with the same limiter and grid level are compared at each shock condition. This indicates the effect of the turbulence model on grid convergence and implies that the magnitudes of numerical errors are influenced by the physical models used.
Error in geometry representation	For the transonic diffuser case, the main source of the discrepancy between the CFD results of the original geometry and the experiment upstream of the shock is the error in the geometry representation. Downstream of the shock, wall pressure results obtained with the same turbulence model and limiter are approximately the same regardless of the geometry used. This may imply that the difference between the experiment and the CFD results downstream of the shock is more likely due to the turbulence models when the finest grid levels are used to minimize the contribution of the discretization error.
Turbulence models	The strong and the weak shock results show that for each flow condition, the highest accuracy in terms of the wall pressure distributions is obtained with a different turbulence model, although the Sp-Al model gives reasonable results for both shock conditions. Uncertainties associated with the turbulence models interact strongly with the discretization errors. In some cases, numerical errors and the physical modelling uncertainties may cancel each other, and the closest results to the experiment can be obtained at intermediate grid levels.
Downstream boundary condition	Changing the location of the exit station or changing the exit pressure ratio affect the strength and the location of the shock. For the strong shock case, the size of the separation bubble is also affected by the same factors.

Table 4: Discretization error results of the transonic diffuser case obtained with the original geometry. The cases presented in this table exhibit monotonic convergence with the refinement of the mesh size. For each case with a different turbulence model, limiter, and exit pressure ratio, the approximation to the exact value of n_{eff} is denoted by $(\tilde{n}_{eff})_{exact}$ and the discretization error at a grid level k is calculated by $error(\%) = \left| \frac{(n_{eff})_k - (\tilde{n}_{eff})_{exact}}{(\tilde{n}_{eff})_{exact}} \times 100 \right|$.

turbulence model	limiter	P_e/P_{0i}	$\tilde{p}$	$(\tilde{n}_{eff})_{exact}$	grid level	discretization error (%)
Sp-Al	Van Albada	0.72	1.528	0.71830	g1	9.820
					g2	4.505
					g3	1.562
					g4	0.542
Sp-Al	Min-Mod	0.72	1.322	0.71590	g1	14.298
					g2	6.790
					g3	2.716
					g4	1.086
Sp-Al	Van Albada	0.82	1.198	0.80958	g1	6.761
					g2	3.507
					g3	1.528
					g4	0.666
Sp-Al	Min-Mod	0.82	1.578	0.81086	g1	8.005
					g2	3.539
					g3	1.185
					g4	0.397
k-ω	Van Albada	0.82	1.980	0.82962	g1	3.514
					g2	1.459
					g3	0.370
					g4	0.094
k-ω	Min-Mod	0.82	1.656	0.82889	g1	4.432
					g2	1.452
					g3	0.461
					g4	0.146

Table 5: Top wall orthogonal distance error $\hat{E}_n$ calculated upstream of the experimental shock location (UESL) for each case obtained with the original geometry. Scaled error values $\hat{E}_n$ were obtained by $\hat{E}_n = \frac{E_n}{(E_n)_{max}} \times 100$ where $(E_n)_{max}$ is the maximum E_n value calculated downstream of the experimental shock location (DESL) for the strong shock case with Grid 4, Min-Mod limiter, and the k-ω turbulence model.

P_e/P_{0i}	Grid	Sp-Al, Min-Mod	Sp-Al, Van Albada	k-ω, Min-Mod	k-ω, Van Albada
0.72	g1	25.6	26.5	27.3	28.2
0.72	g2	23.5	24.0	26.1	25.8
0.72	g3	23.9	24.0	26.3	26.2
0.72	g4	25.8	23.8	27.3	27.1
0.82	g1	27.3	29.3	28.9	31.1
0.82	g2	27.1	27.5	28.0	28.4
0.82	g3	27.7	27.8	28.4	28.5
0.82	g4	27.6	27.6	28.2	28.2

Table 6: Top wall orthogonal distance error $\hat{E}_n$ calculated downstream of the experimental shock location (DESL) for each case obtained with the original geometry.

P_e/P_{0i}	Grid	Sp-Al, Min-Mod	Sp-Al, Van Albada	k-ω, Min-Mod	k-ω, Van Albada
0.72	g1	81.2	64.4	85.6	74.6
0.72	g2	52.3	48.9	89.9	83.7
0.72	g3	35.0	34.5	90.1	89.2
0.72	g4	27.8	27.9	100.0	97.8
0.82	g1	27.1	21.4	14.6	14.6
0.82	g2	11.3	10.9	14.6	14.3
0.82	g3	17.7	16.9	12.9	13.3
0.82	g4	21.2	20.8	10.8	10.7

Table 7: Nozzle efficiency values obtained with different grid levels, limiters, turbulence models, geometries, and boundary conditions.

turbulence model	limiter	grid level	strong shock				weak shock			
			original geometry	*modified-wall geometry*	*extended geometry*		*original geometry*	*modified-wall geometry*	*extended geometry*	
					P_e/P_{0i} 0.7468	P_e/P_{0i} 0.72			P_e/P_{0i} 0.8368	P_e/P_{0i} 0.82
k-w	Min-mod	1	0.81113	0.80556			0.86563	0.86158		
		2	0.79362	0.79640			0.84093	0.83297		
		3	0.78543	0.78886			0.83271	0.82249		
		4	0.79007				0.83011			
k-w	Van Albada	1	0.78820	0.78333			0.85879	0.84477		
		2	0.78199	0.78439			0.84174	0.83420		
		3	0.78310	0.78661			0.83270	0.82237		
		4	0.78788				0.83041			
Sp-Al	Min-mod	1	0.81827	0.81562			0.87577	0.86931		
		2	0.76452	0.76479			0.83956	0.83290		
		3	0.73535	0.73402			0.82048	0.81409		
		4	0.72369				0.81408			
Sp-Al	Van Albada	1	0.78885	0.78647	0.78855	0.77702	0.86432	0.85336	0.89069	0.85429
		2	0.75067	0.74850	0.75777	0.75072	0.83797	0.83172	0.87461	0.82993
		3	0.72953	0.72569	0.74231	0.73526	0.82195	0.81586	0.86819	0.81664
		4	0.72220		0.73268	0.72517	0.81497		0.86464	0.81130

Table 8: Main observations on the uncertainty in nozzle efficiencies

Shock type	Observations on uncertainties
Strong shock case	The range of variation in nozzle efficiency results is much larger than that observed in the weak shock case. The maximum variation is about 10% for the strong shock case, and 4% for the weak shock case, when the results of the original geometry are compared.
	Magnitude of the discretization errors is larger than that of the weak shock case. The discretization errors at grid level 2 can be up to 6% for the strong shock case.
	Relative uncertainty due to the selection of the turbulence model can be larger than that due to discretization errors depending upon the grid level used. This uncertainty can be as large as 9% at grid level 4.
	The contribution of the error in geometry representation to the overall uncertainty is negligible compared to the other sources of uncertainty.
Weak shock case	Discretization error is the dominant source of uncertainty. The maximum value of the discretization error is 3.5%, whereas the maximum value of turbulence model uncertainty is about 2%.
	The nozzle efficiency values are more sensitive to the exit boundary conditions and associated error magnitudes can be larger than from other sources. The difference between the results from original geometry and the extended geometry can be as large as 7% when the exit pressure ratio of 0.8368 is used.
	The contribution of the error in geometry representation to the overall uncertainty can be up to 1.5%.

Table 9: Discretization errors calculated by using the results of different grid levels for the transonic diffuser case with the original geometry, Sp-Al turbulence model, and the Min-Mod limiter.

grid levels used	$\tilde{p}$	$(\tilde{n}_{eff})_{exact}$	grid level	error (%)
for $\tilde{p}$: g2, g3, and g4 for $(\tilde{n}_{eff})_{exact}$: g3 and g4	1.322	0.71590	g1	14.298
			g2	6.790
			g3	2.716
			g4	1.086
			g5	0.634
for $\tilde{p}$: g3, g4, and g5 for $(\tilde{n}_{eff})_{exact}$: g4 and g5	1.849	0.71921	g1	13.774
			g2	6.300
			g3	2.245
			g4	0.623
			g5	0.173

Table 10: Discretization error results of the RAE 2822 airfoil cases.

case	observed order of accuracy	grid level	mesh size	CL	discretization error (%)
Mach = 0.3 $\alpha = 0.0$ degrees $Re = 6.2 \times 10^6$	2.140	1	92×16	0.1594	22.430
		2	184×32	0.1969	4.166
		3	368×64	0.2055	0.021
		4	736×128	0.2055	0.005
Mach = 0.75 $\alpha = 3.19$ degrees $Re = 6.2 \times 10^6$	1.127	1	92×16	0.6899	14.369
		2	184×32	0.7509	6.794
		3	368×64	0.7789	3.326
		4	736×128	0.7934	1.522
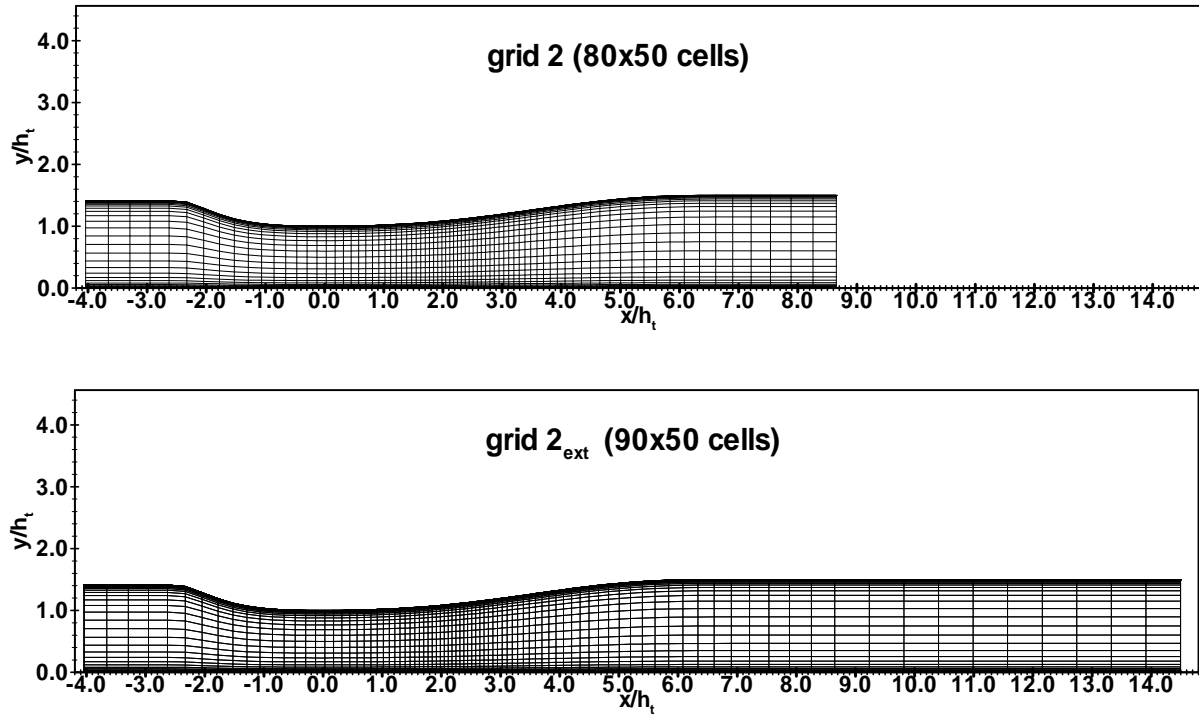
Figure 1: Original geometry, Grid 2 (top), and extended geometry, Grid 2_{ext} (bottom), used in the transonic diffuser computations. The flow is from left to right, in the positive x-direction. The y-direction is normal to the bottom wall. All dimensions are scaled by the throat height, h_t. The throat section, which is the minimum cross-sectional area of the channel, is located at $x/h_t = 0.0$. Both geometries have the inlet stations located at $x/h_t = -4.04$.
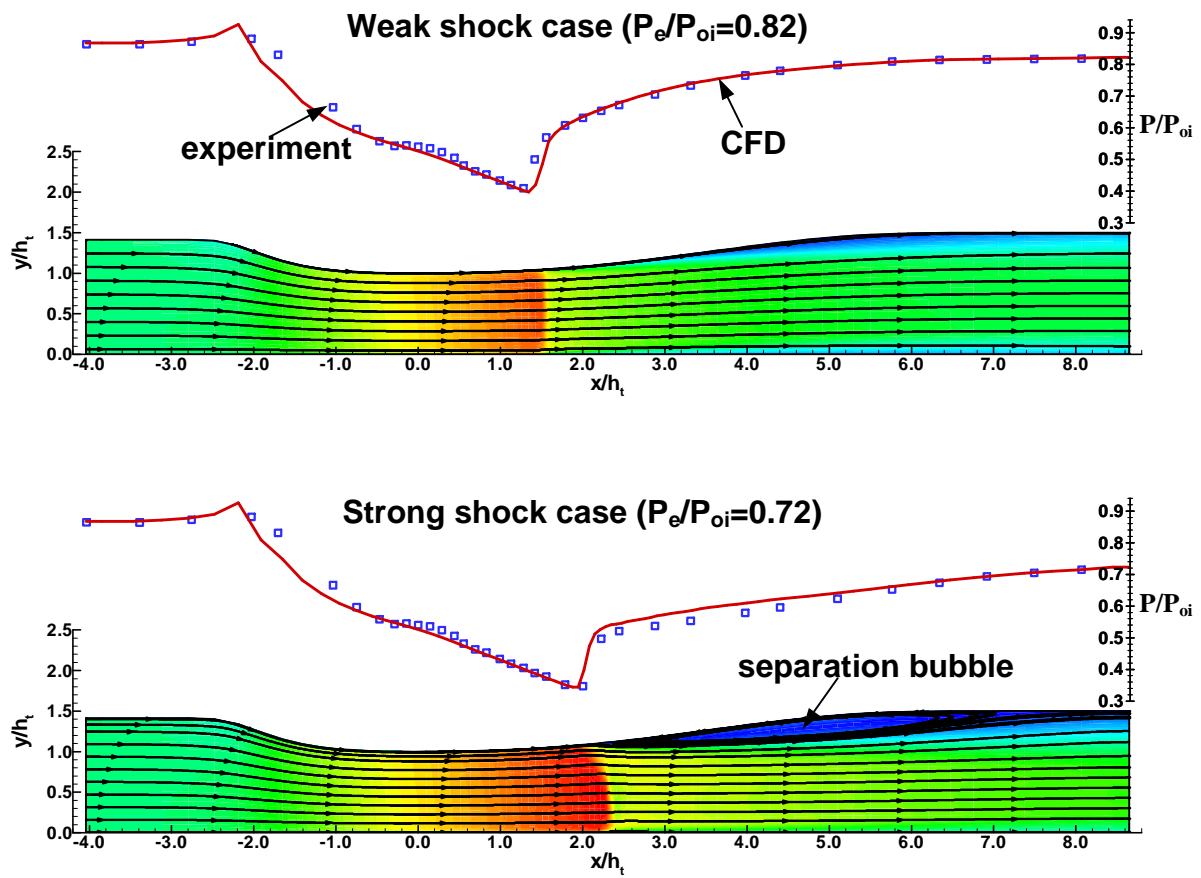
Figure 2: Velocity contours, streamlines, and the top wall pressure distributions of the weak and the strong shock cases.
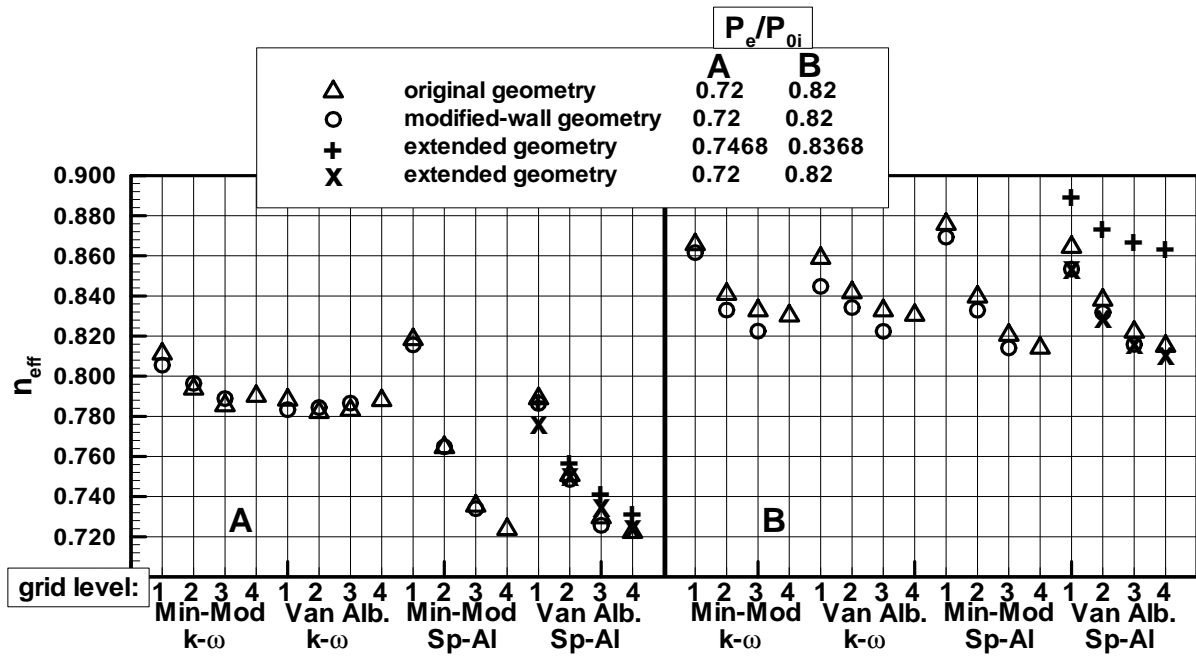
Figure 3: Nozzle efficiencies obtained with different grid levels, turbulence models, limiters, geometries, and boundary conditions for the strong shock case (A) and the weak shock case (B).
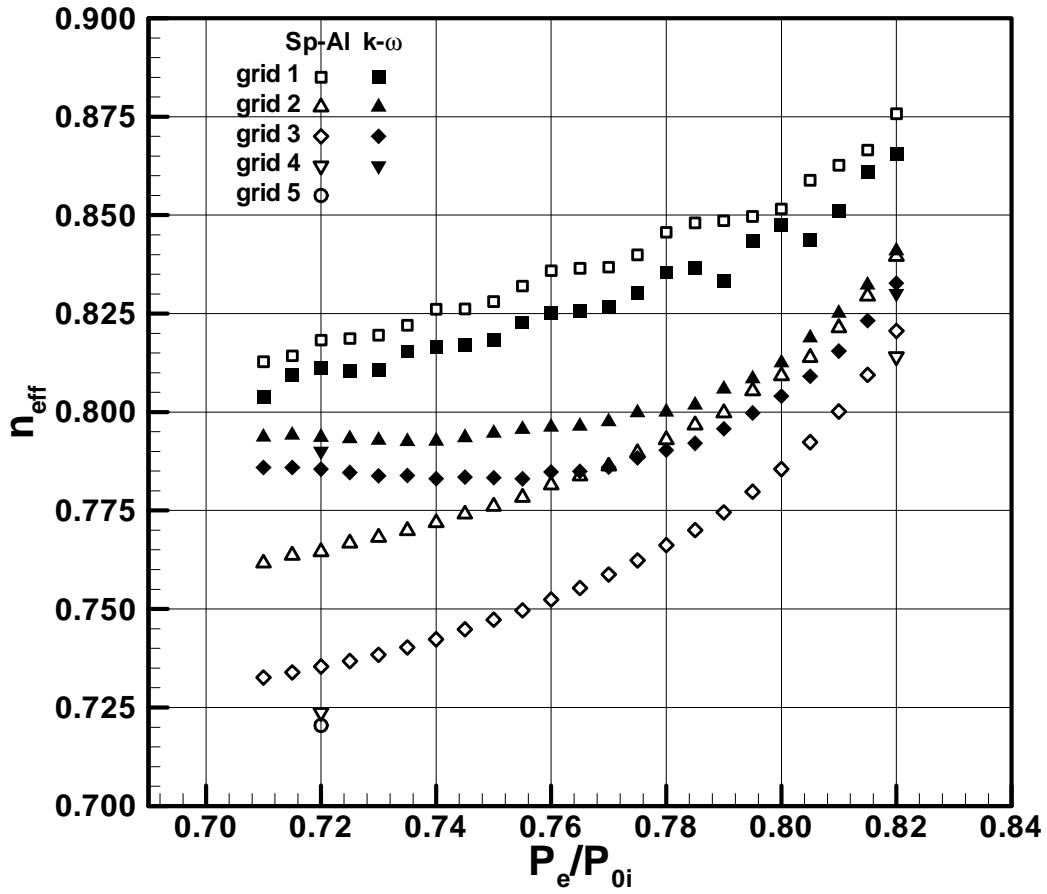
Figure 4: Nozzle efficiency vs. exit pressure ratio for different grids obtained with the original geometry, Sp-Al and k-ω turbulence models, and the Min-Mod limiter.
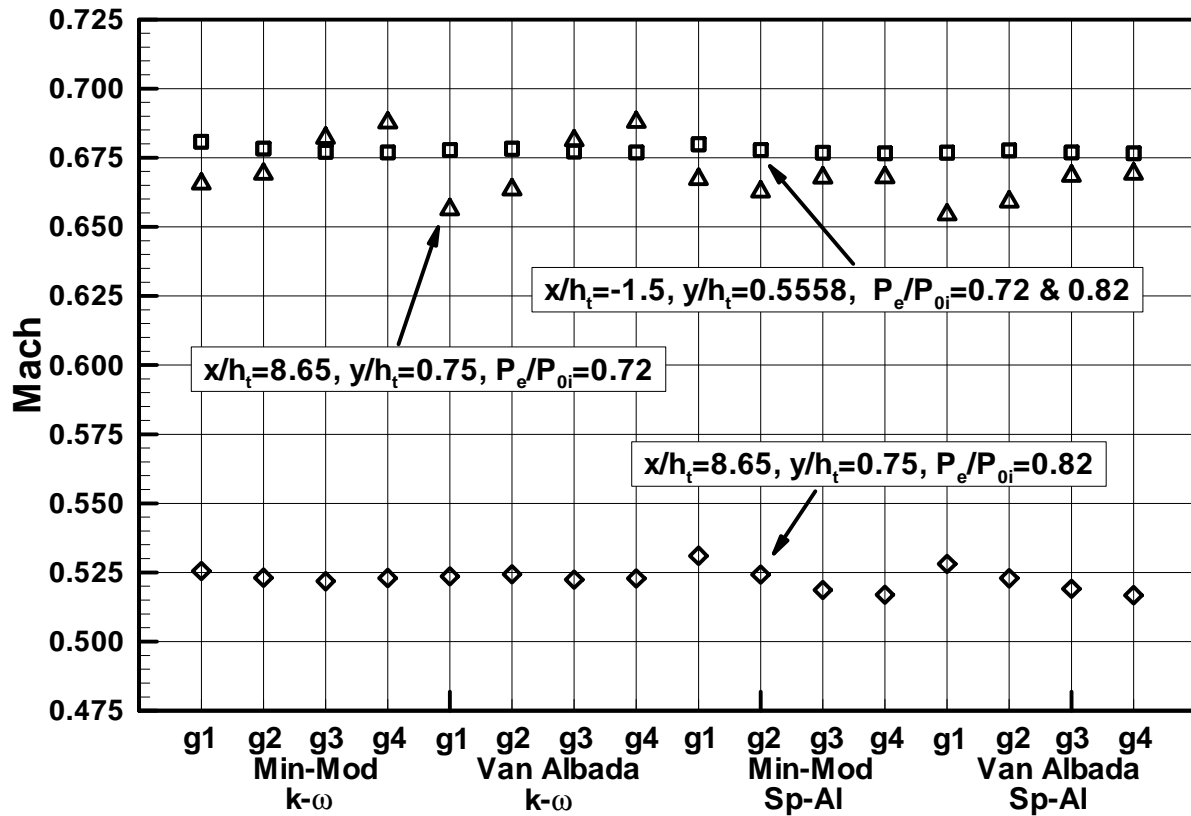
Figure 5: Mach number values at the upstream of the shock ($x/h_t = -1.5$), and downstream of the shock ($x/h_t = 8.65$, the exit plane) for different grids obtained with the original geometry, Sp-Al and k-ω turbulence models, Min-Mod and Van Albada limiters. The values of y/h_t correspond to the mid points of the local channel heights.
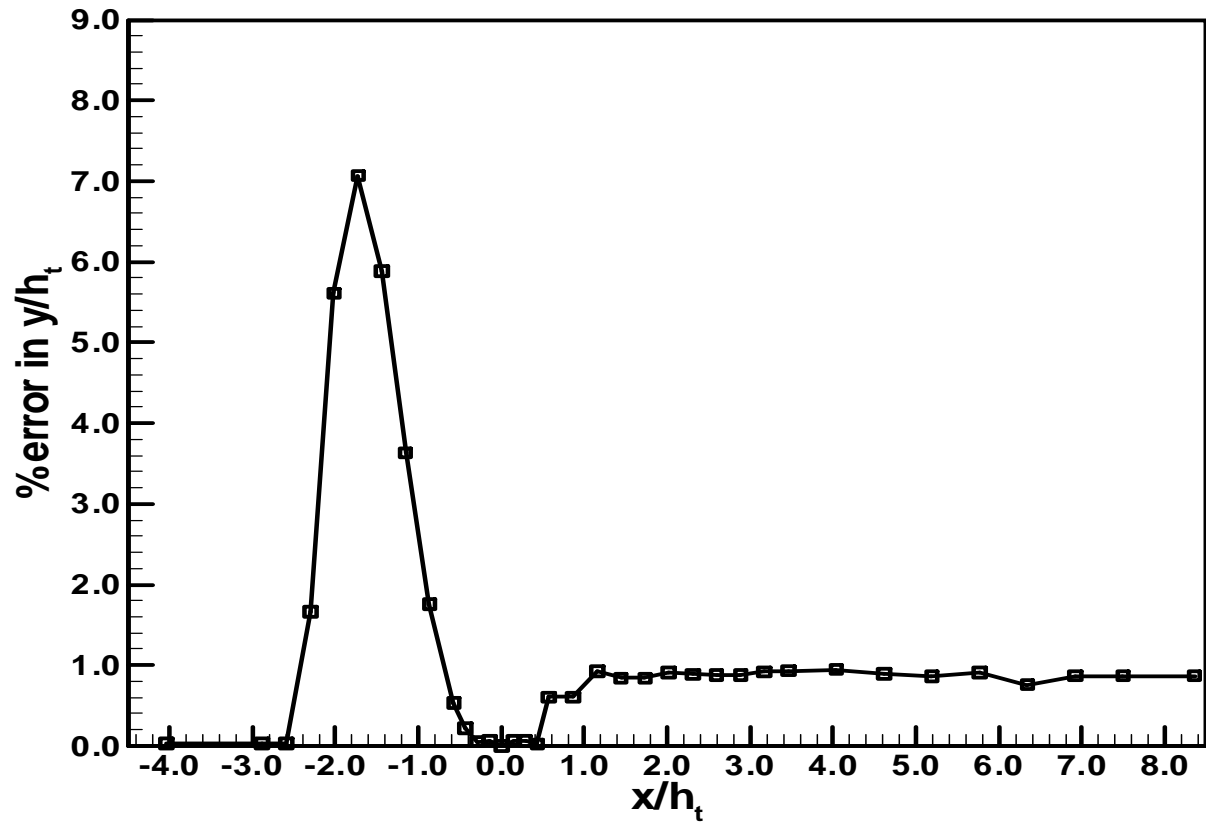
Figure 6: Error distribution in y/h_t for the upper wall of the modified-wall diffuser geometry at the data points measured in the experiments. The maximum error is approximately 7% and observed upstream of the throat, at $x/h_t = -1.95$. Starting from $x/h_t = 1.2$, the error is approximately constant with an average value of 0.9%.
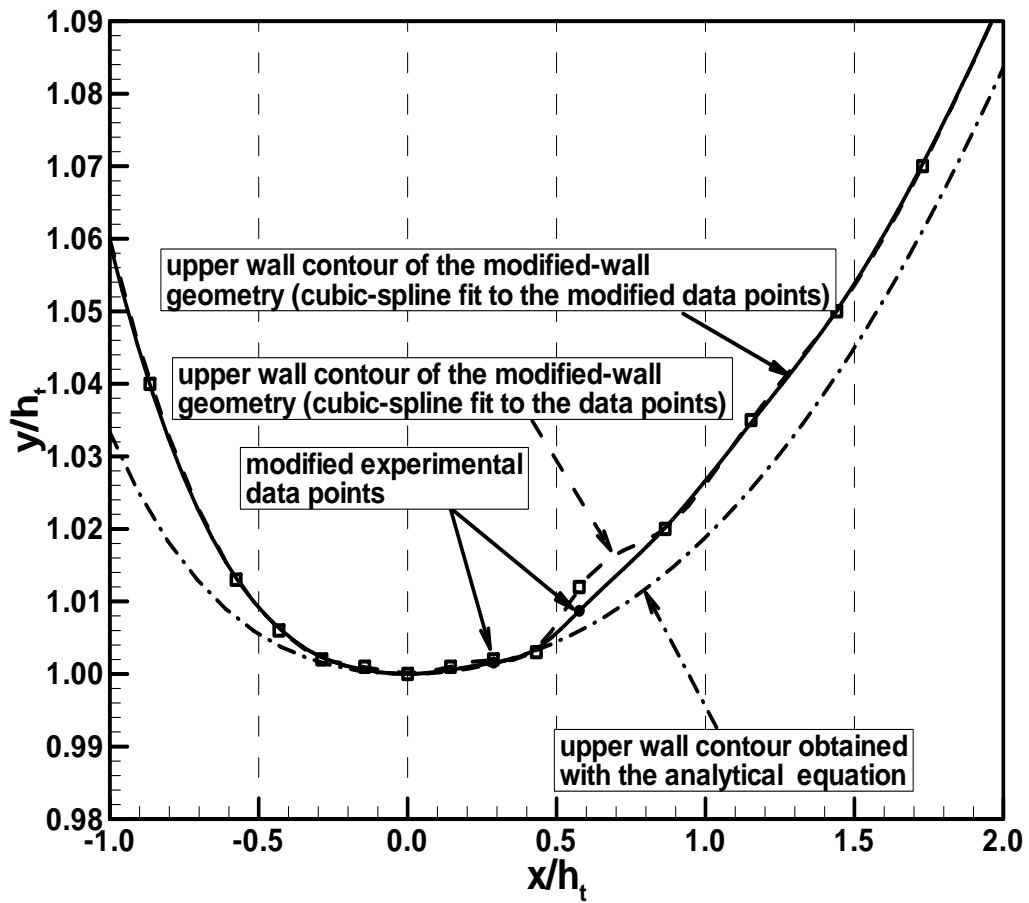
Figure 7: Upper wall contours of the original and the modified-wall diffuser geometry in the vicinity of the throat location.
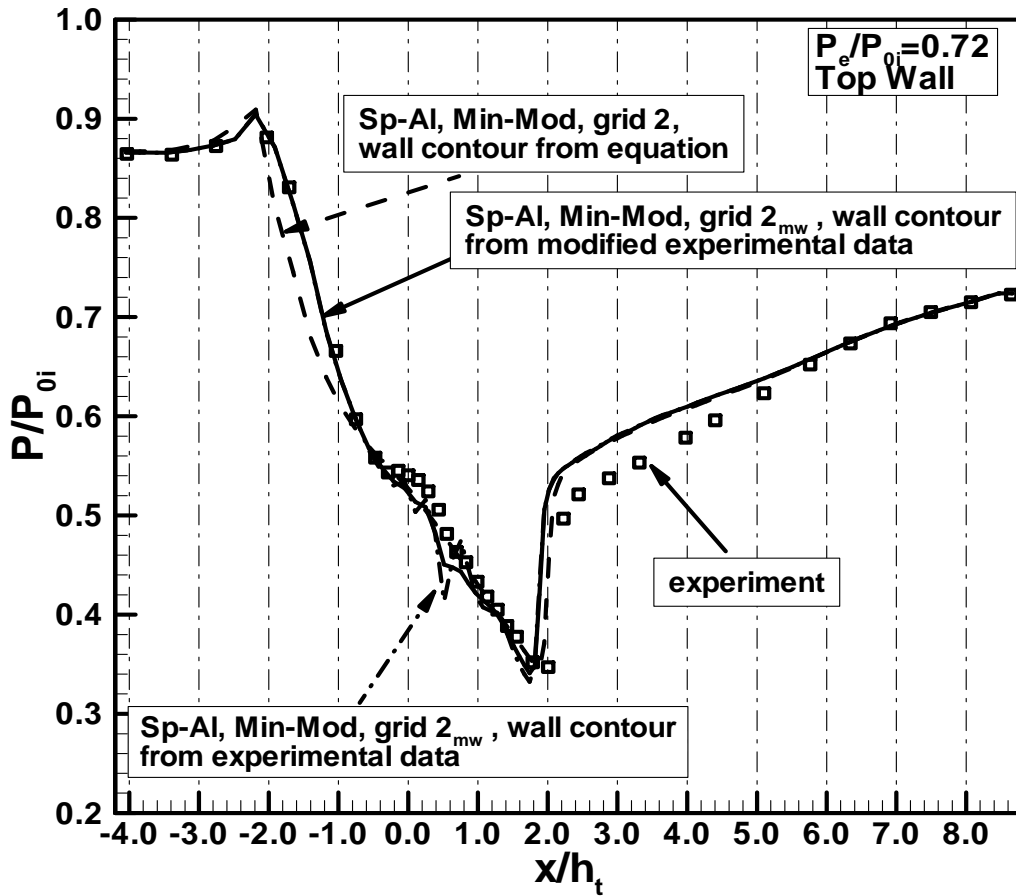
Figure 8: Top wall pressure distributions obtained with the original and the modified-wall geometry for the strong shock case (the results of the Sp-Al model, Min-Mod limiter, and Grids g2 and g2$_{mw}$ are shown).
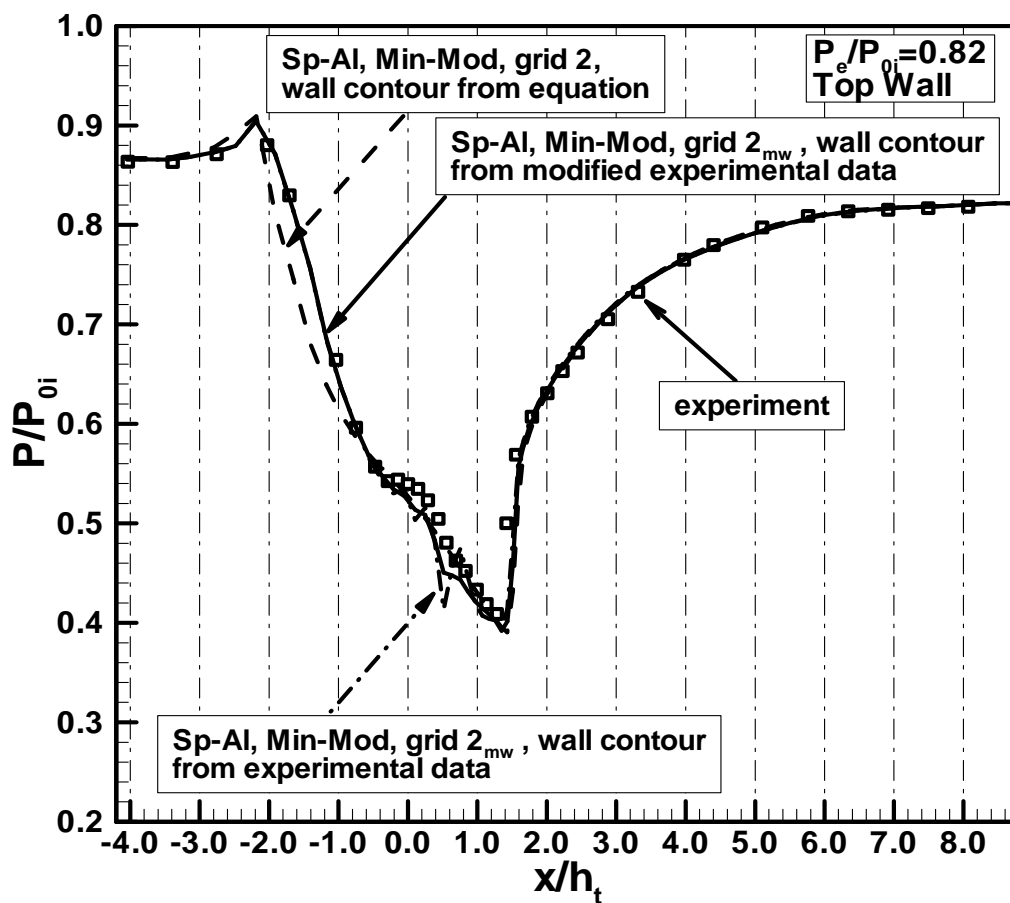
Figure 9: Top wall pressure distributions obtained with the original and the modified-wall geometry for the weak shock case (the results of the Sp-Al model, Min-Mod limiter, and Grids g2 and $g2_{mw}$ are shown).
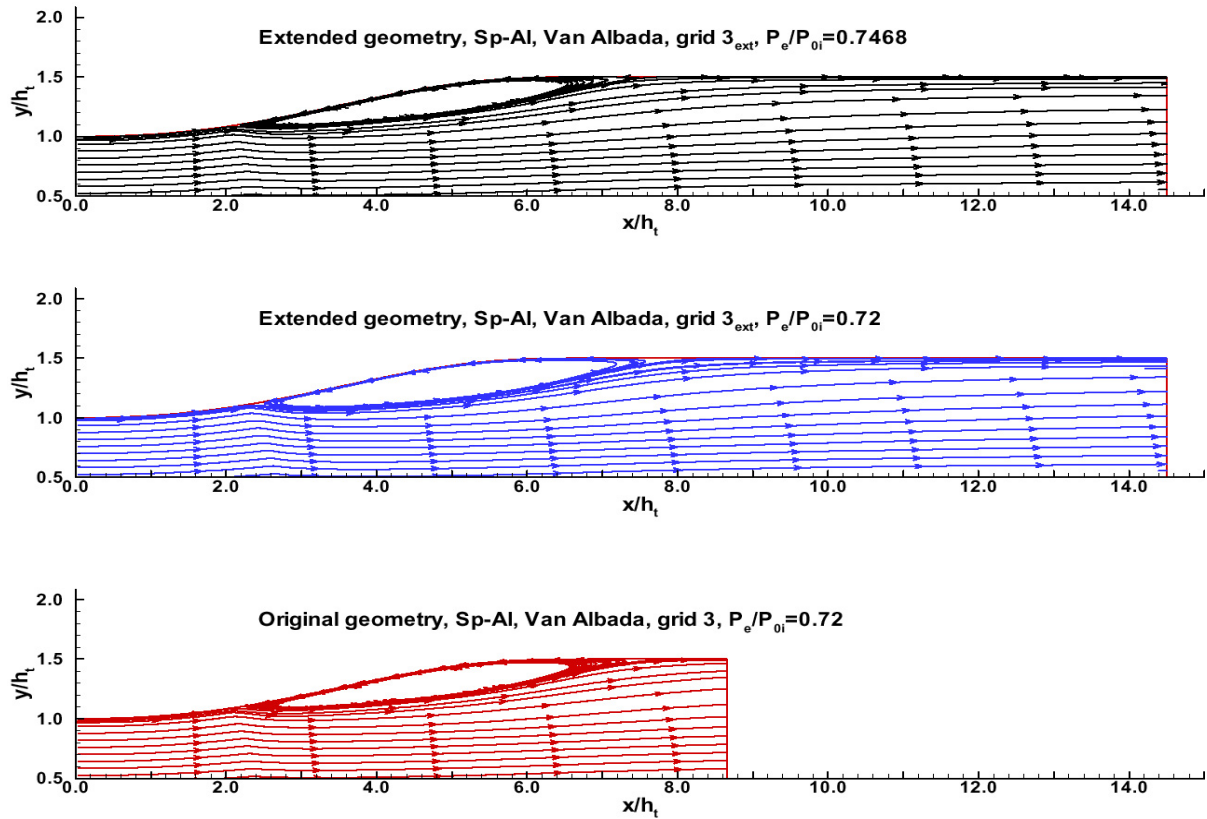
Figure 10: Streamline patterns of the separated flow region obtained with different versions of the diffuser geometry and exit pressure ratios for the strong shock case.
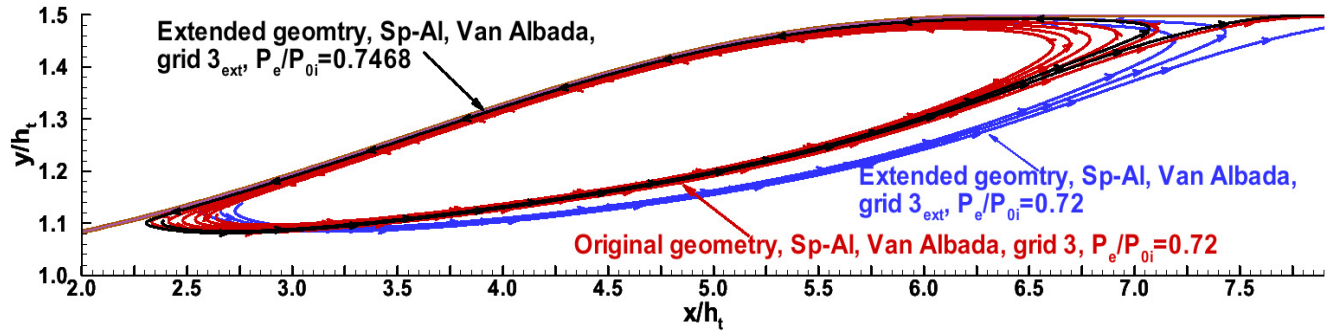
Figure 11: Comparison of the separation bubbles obtained with different versions of the diffuser geometry and exit pressure ratios for the strong shock case.
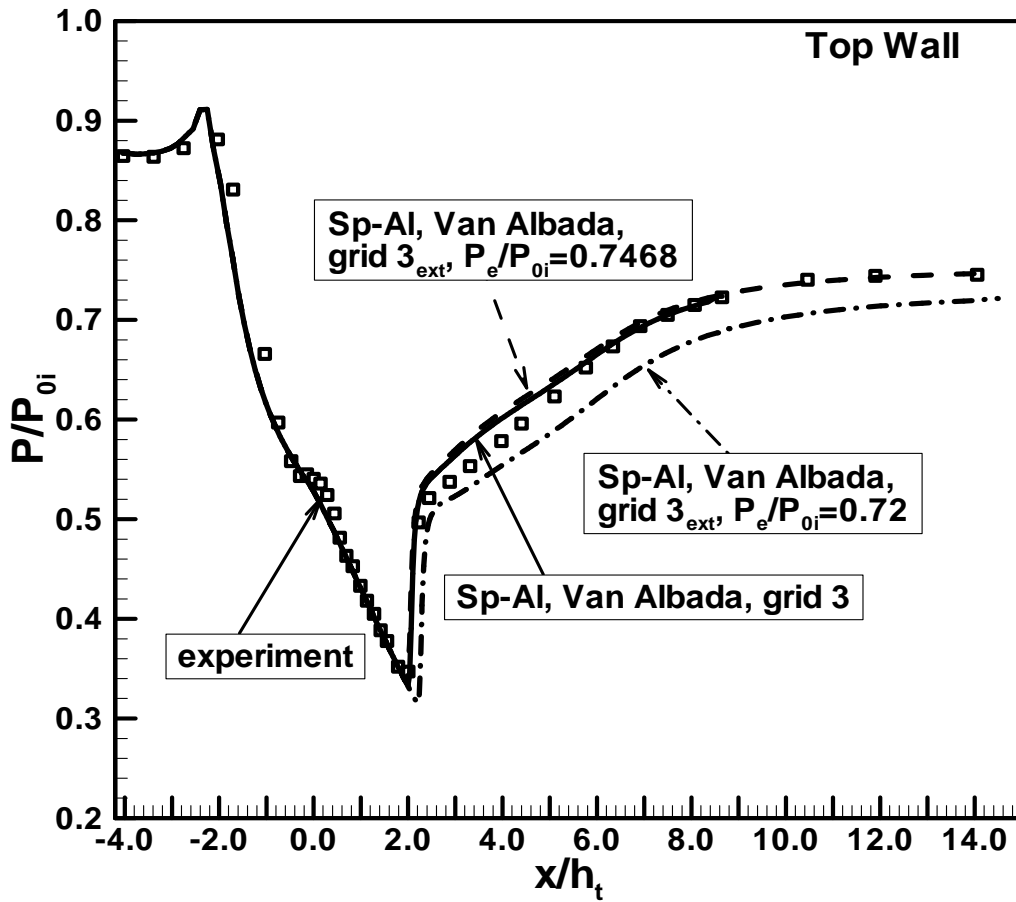
Figure 12: Top wall pressure distributions obtained with different versions of the diffuser geometry and exit pressure ratios for the strong shock case (the results of the Sp-Al model, Van Albada limiter, and Grids g3 and g3$_{ext}$ are shown).
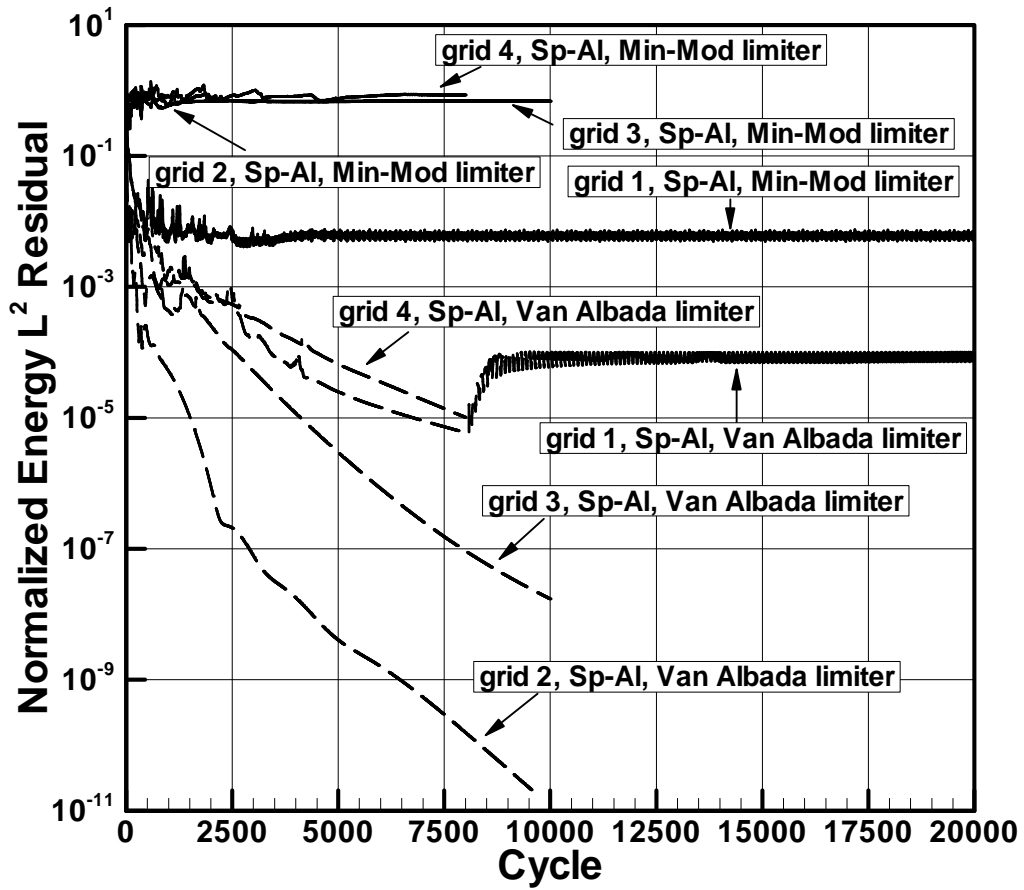
Figure 13: Normalized L^2 residual of the energy equation for the case with the Sp-Al turbulence model, Van Albada, and Min-Mod limiters at $P_e/P_{0i} = 0.72$ obtained with the original geometry. Normalization is done with the initial value of the residual.
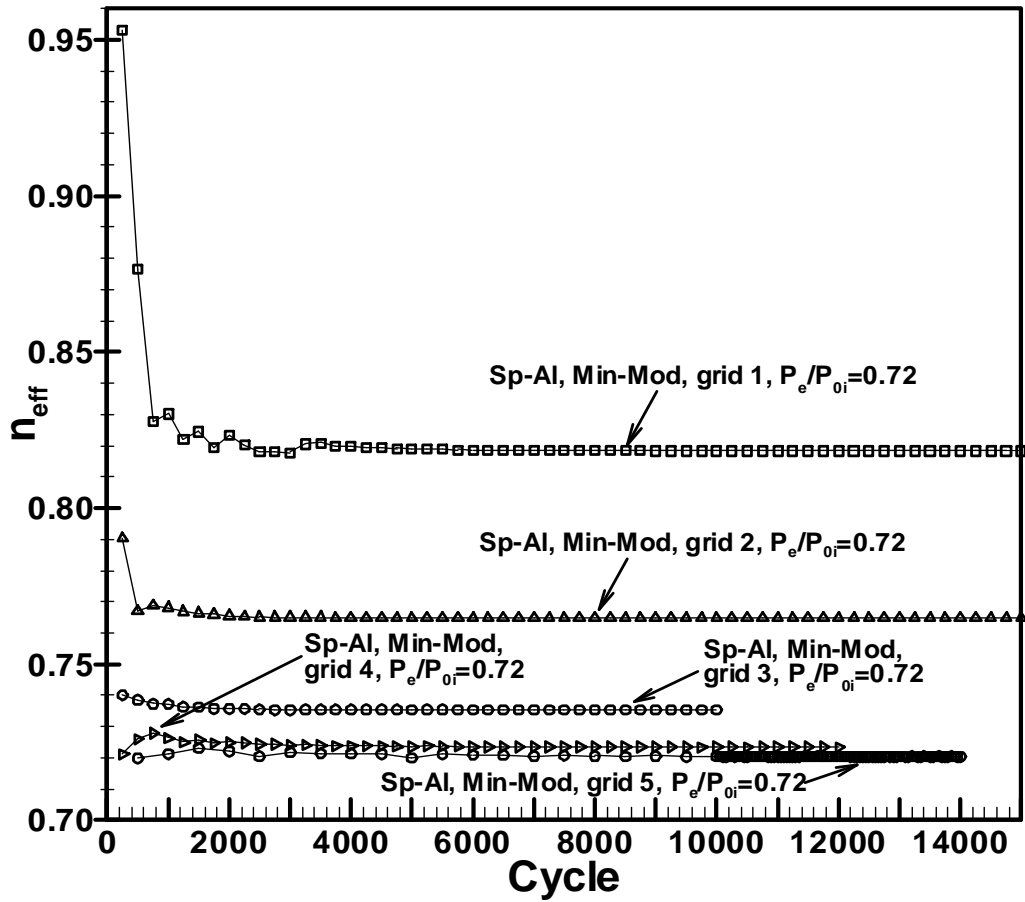
Figure 14: Convergence history of the nozzle efficiency at different grid levels for the Sp-Al, Min-Mod, strong shock case obtained with the original geometry. (The nozzle efficiency values are monitored at every 50 cycles starting from iteration number 10000 for Grid 5)

67
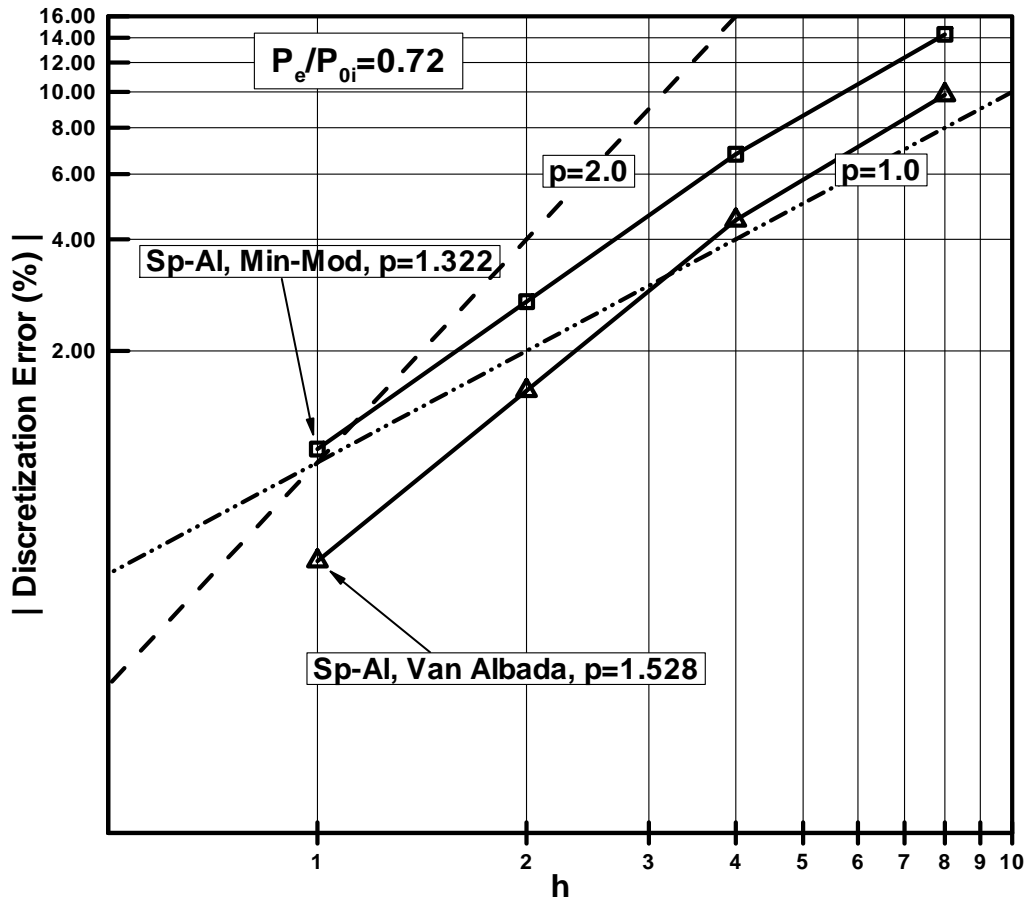
Figure 15: Absolute value of the discretization error (%) vs. h for the cases with the Sp-Al turbulence model, Van Albada, and Min-Mod limiters at $P_e/P_{0i} = 0.72$ obtained with the original diffuser geometry.
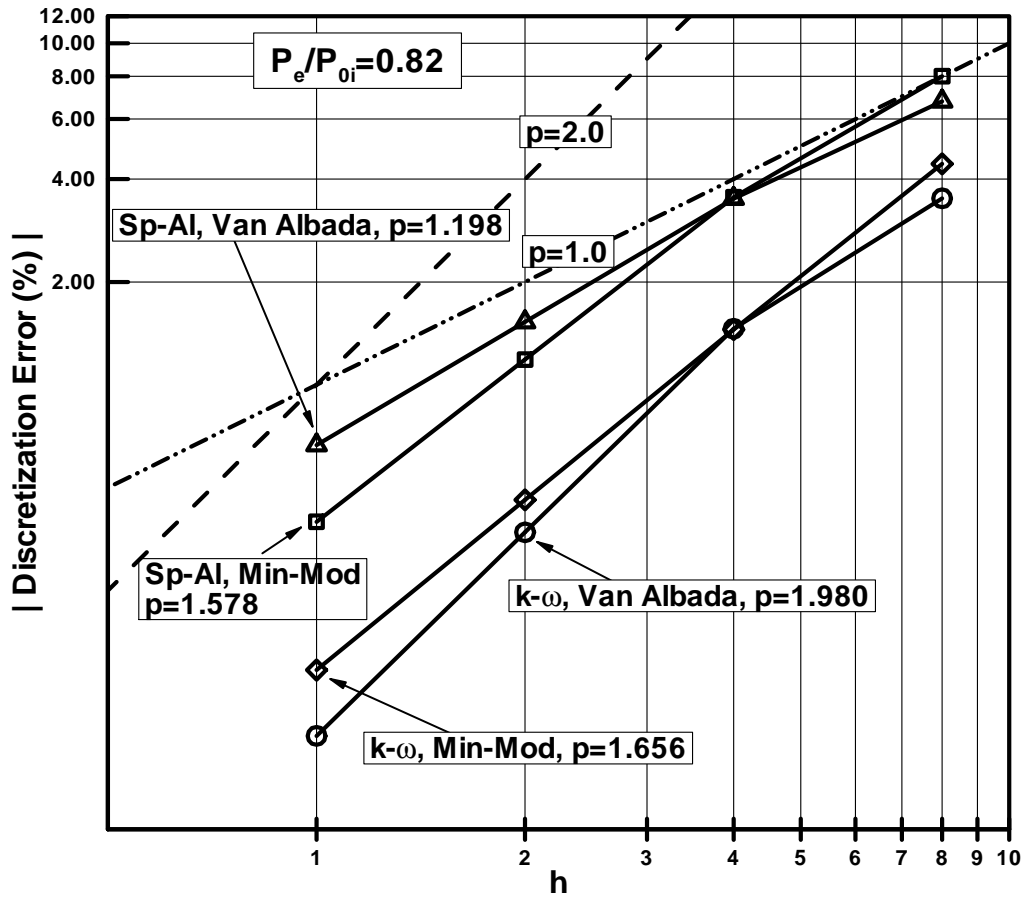
Figure 16: Absolute value of the discretization error (%) vs. h for the cases with Sp-Al and k-ω turbulence models, Van Albada, and Min-Mod limiters at $P_e/P_{0i} = 0.82$ obtained with the original diffuser geometry.
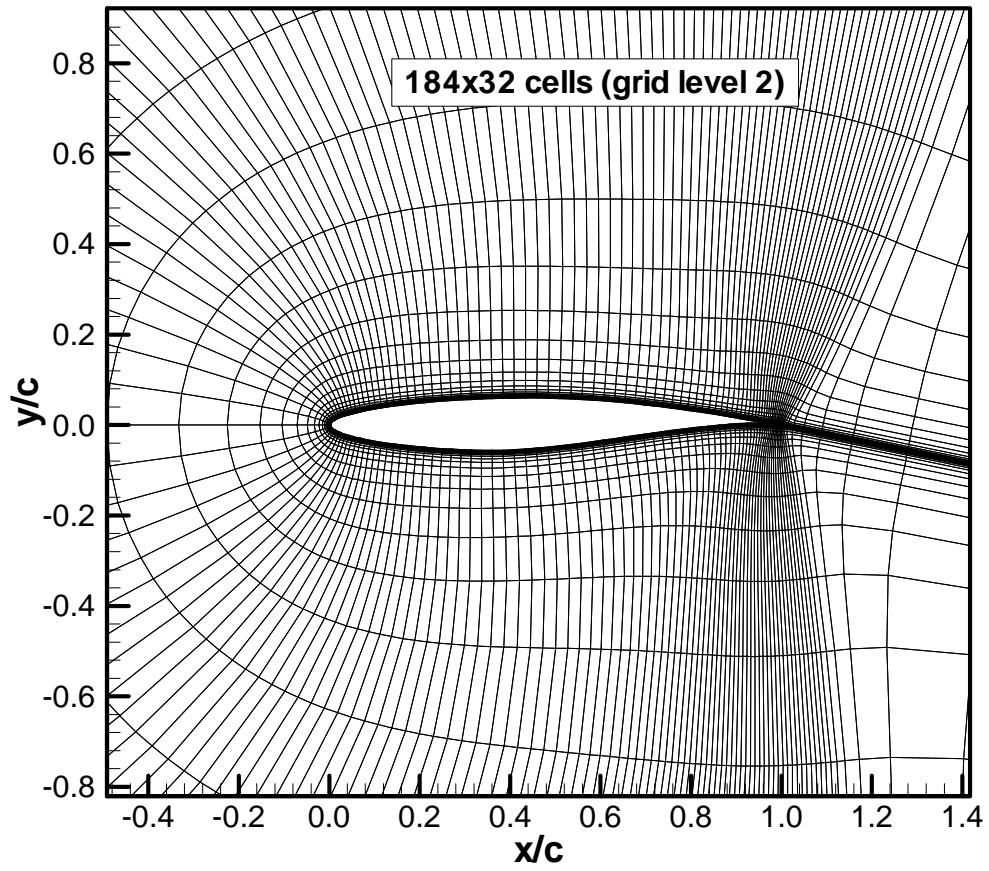
69

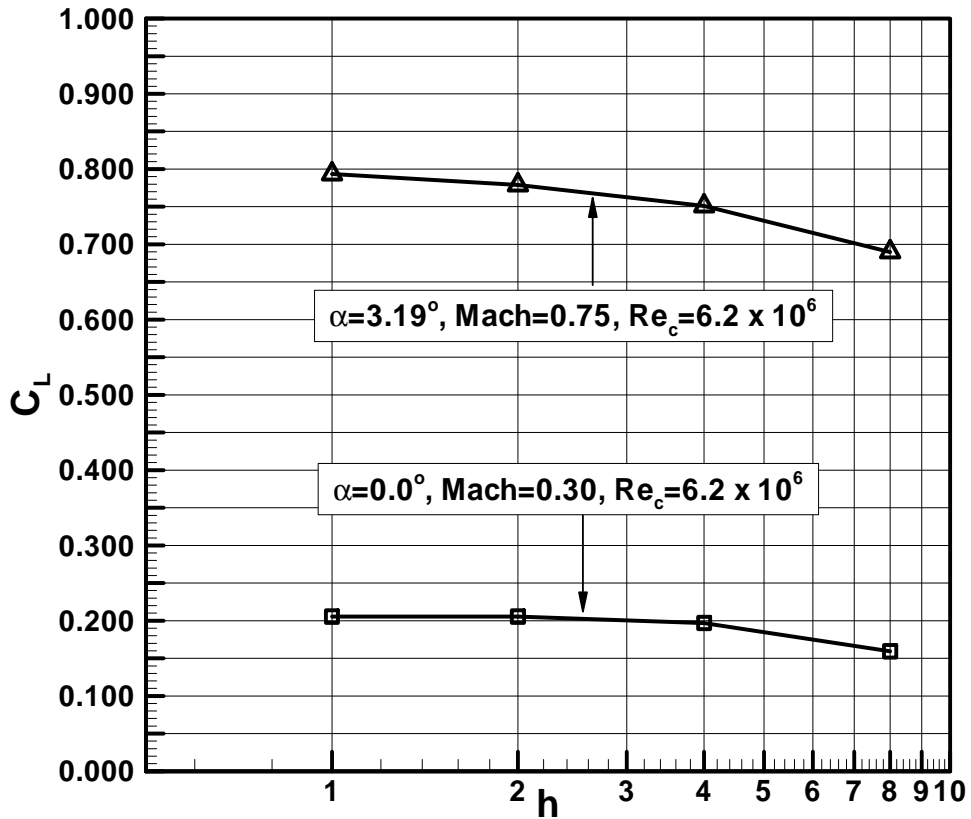Figure 17: Grid level 2 (184×32) used in the RAE 2822 airfoil calculations.

Figure 18: Logarithmic plot of CL vs. h (measure of grid spacing) for the RAE 2822 airfoil cases.